# Ionic and Neutral Species in Pulse Radiolysis of Supercritical $CO_2$. 1. Transient Absorption Spectroscopy, Electric Field Effect, and Charge Dynamics

**Ilya A. Shkrob,* Myran C. Sauer, Jr., Charles D. Jonah, and Kenji Takahashi†**

*Chemistry Division, Argonne National Laboratory, Argonne, Illinois 60439*

*Received: June 25, 2002; In Final Form: August 22, 2002*

Transient absorption spectroscopy was used to study the mechanism for radiolysis of dense, liquidlike supercritical (sc) $CO_2$ ($T = 41$ °C, $\rho = 0.84$ g/cm$^3$). The 350−1500 nm spectra are decomposed into the contributions from the solvent radical cation, solvent radical anion, and a long-lived neutral product that we associate with singlet carbon trioxide, $CO_3(^1A_1)$. These three species are characterized by their optical spectra, chemical behavior, kinetics, and the response of these kinetics to external electric field. The following mechanism for radiolysis of sc $CO_2$ is suggested: Ionization of the solvent yields ≈5 pairs per 100 eV. Most of these pairs are comprised of the solvent hole and a thermalized quasifree electron; the prompt yield of $CO_3^-$ is <3% of the total ion yield. The electrons are trapped by the solvent in <200 ps. Because of high electron mobility, most of this trapping occurs after the charges escape each other's Coulomb field. Because of cross recombination of the electrons with nongeminate solvent holes, the lifetime of the quasifree electrons is further reduced. A theoretical model that accounts for these dynamics is suggested. It is shown that di- and triatomic molecules donate an electron to the solvent hole, and the resulting solute cations polymerize. Exotic ion species, such as $(N_2O)_2^+$ and $(CO)_n^+$, can be produced this way. Using sc $CO_2$ provides an opportunity to study such multimer cations in liquid solution.

## 1. Introduction

Having a critical density $\rho_c$ of 0.468 g/cm$^3$ and a critical temperature $T_c$ of 31 °C, supercritical carbon dioxide (sc $CO_2$) is a convenient, environment-friendly solvent for industrial applications. Unfortunately, using this solvent for organic synthesis is still a matter of trial and error because the reaction mechanisms in supercritical fluids are poorly understood. Many of these reactions involve short-lived intermediates, such as carbonium cations. For some of these, pulse radiolysis is the only practical way to generate sufficient concentrations of the species to observe their dynamics by transient absorption spectroscopy on a short time scale. For that and other reasons, the mechanism for radiolysis of sc $CO_2$ is of considerable interest. In recent studies from this laboratory, pulse radiolysis−transient absorption spectroscopy[1−3] and laser-induced dc conductivity[4] have been used to unravel the chemistry occurring after the ionization of supercritical $CO_2$ solutions.

Two species were observed shortly after a 5 ns fwhm pulse of 20 MeV electrons.[1,2,3] One of these species is the solvent radical cation (also referred to as "solvent hole" and $(CO_2)_n^+$) whose bell-shaped 750 nm band extends over the whole visible region (Figure 2 in ref 1). The assignment of this band to the cation was suggested by the fact that addition of electron scavenger ($SF_6$) *increases* the yield of the 750 nm band (Figure 4 in ref 1), whereas pressurizing the solvent *decreases* this yield (Figure 5 in ref 1). The latter trend is consistent with a lower free cation yield because of a decrease of the thermalization path of electrons at higher density. The solvent cation in sc $CO_2$ rapidly reacts, by charge transfer, with electron donors, such as aromatic amines,[1,2] CO,[2] and $O_2$,[2] and abstracts a proton from $H_2$.[3] Because of rapid scavenging by impurity, a typical half-time for the decay of the 750 nm band is <100 ns.[1−3] Apart from the solvent radical cation, Takahashi et al.[3] observed another species, with a longer lifetime, that absorbed at 400−600 nm. This species was identified as the solvent radical anion, $(CO_2)_n^-$, which seemed consistent with the data on radiolysis of $O_2$ and $H_2$ solutions in sc $CO_2$ (see ref 3 for more detail).

The presence of $(CO_2)_n^-$ in the reaction mixture was also suggested by delayed generation of *p*-benzoquinone anion ($BQ^-$) in radiolyzed *p*-benzoquinone solution.[2] Apart from this delayed formation, 50−80% of $BQ^-$ was formed within the duration of a 5 ns fwhm pulse.[2] Prompt formation of $BQ^{-2}$ and a large effect of $SF_6$ on the solvent radical cation yield[1] suggest that the solvent radical anion has a short-lived, mobile, reactive precursor. In this work, we demonstrate that this precursor is a metastable quasifree electron ($e_{qf}^-$). This conclusion is in accord with a time-resolved dc photoconductivity study of Shkrob and Sauer[4] that demonstrated the involvement of $e_{qf}^-$ in the multiphoton ionization of aromatic hydrocarbons in sc $CO_2$. According to their study, the recombination dynamics in dense sc $CO_2$ ($\rho/\rho_c > 1.2$) occurs in two distinct stages. In the first few hundred picoseconds after the ionization event, the excess negative charge is present as a conduction band electron, $e_{qf}^-$, that has high mobility ($\mu_e \sim 10-100$ cm$^2$/Vs) and short "natural" lifetime $\tau_e$ (<200 ps). The lifetime-mobility product $\mu_e\tau_e$ exponentially increases with solvent density $\rho$ for $1.2 < \rho/\rho_c < 2$ and approaches $2.5 \times 10^{-9}$ cm$^2$/V for $\rho = 0.84$ g/cm$^3$ and $T = 41$ °C. After the electrons are trapped by the solvent, a long-lived (>10 $\mu$s) solvent radical anion, $(CO_2)_n^-$, is formed, which has a mobility of $1.6 \times 10^{-2}$ cm$^2$/Vs (under the same conditions). This anion migrates by charge hopping that accelerates as the solvent density increases. It has 3−10 times greater mobility than any other ion in sc $CO_2$.[4] Temperature

* To whom correspondence should be addressed. Phone: 630-2529516. Fax: 630-2524993. E-mail: shkrob@anchim.chm.anl.gov.

† Permanent Address: Division of Quantum Energy Engineering, Graduate School of Engineering, Hokkaido University, Sapporo 060-8628, Japan.

10.1021/jp021494k CCC: $22.00 
Published on Web 11/07/2002

and pressure dependencies for the mobilities of the electron,[4] solvent radical anion,[4] and secondary ions (such as $F^-$ and $CO_4^-$)[4,5] were determined. Reactions of $e_{qf}^-$ and $(CO_2)_n^-$ with various electron acceptors were studied and the electron photodetachment spectrum of $(CO_2)_n^-$ was obtained.[4] This spectrum is similar to the photoelectron spectra of multimer $(CO_2)_n^-$ anions ($n > 6$) in the gas phase;[6] it is different from the photodetachement spectrum of $CO_2^-$ in hydrocarbon liquids.[7] For the solvent radical anion in sc $CO_2$, the onset of electron photodetachment is at 1.76 eV[4] (vs 1 eV for $CO_2^-$ in isooctane);[7] that is, the electron is deeply trapped by sc $CO_2$. Deep trapping is also suggested by the fact that only solutes with gas-phase electron affinity >2 eV exhibit diffusion-controlled rates of reaction with $(CO_2)_n^-$.[4] Gas-phase studies of Johnson and co-workers[6] suggest that a C−C bonded, $D_{2d}$ symmetric $(CO_2)_2^-$ dimer[6,8,9] is the core anion in the $(CO_2)_n^-$ clusters ($n > 14$).

The blue-absorbing species observed by Takahashi et al.[3] (that was associated with the solvent anion) exhibits a spectrum that is quite different from the photodetachment spectrum of $(CO_2)_n^-$ obtained in ref 4. Furthermore, this species was found to react differently from the $(CO_2)_n^-$ anions observed in the photoconductivity studies. In this work, selective scavenging and transient absorption spectroscopy in the presence of an electric field were used to separate spectral contributions from the light-absorbing species generated in pulse radiolysis of sc $CO_2$. The "solvent anion" observed by Takahashi et al.[3] is shown to be a neutral product with a lifetime >300 ms. This product is formed on the time scale of ion recombination, over tens of nanoseconds. Several possible candidates for this product are examined, and $CO_3(^1A_1)$ is suggested as the most likely one. In addition to this product, the solvent radical anion was observed shortly after the electron pulse and shown to have the same absorption spectrum as the $(CO_2)_n^-$ species observed in the conductivity experiments of Shkrob and Sauer.[4] The absorption spectrum of $(CO_2)_n^+$ in the 350−1500 nm region was obtained and the extinction coefficient and the oscillator strength of the corresponding electron transition determined. The nature of the solvent radical cation and the solvent radical anion in sc $CO_2$ is further discussed in Part 2 of this work.[10]

In sc $CO_2$, electron attachment to the solvent could be either dissociative (with the formation of CO and $O^-$) or nondissociative (with the formation of the $(CO_2)_n^-$ anion), depending on the electron energy. The $O^-$ anion very rapidly attaches to $CO_2$ yielding a carbonate radical anion, $CO_3^-$.[11−13] Though the dissociative attachment requires ≈3.6 eV higher energy (as determined for gas-phase $(CO_2)_2$ clusters),[11] a significant fraction of prethermalized electrons generated in radiolysis of sc $CO_2$ have energies of 10−20 eV. The involvement of $CO_3^-$ in the radiolysis and laser photolysis of gaseous $CO_2$ and $O_2$:$CO_2$ mixtures has been postulated by several authors.[12] Furthermore, the trapped $CO_3^-$ radical was observed, by EPR spectroscopy, in $\gamma$-irradiated solid $CO_2$ at 77 K.[13] Although the formation of $CO_3^-$ in radiolysis of sc $CO_2$ is likely, no clear spectroscopic evidence for the formation of this species was obtained. In this work, an upper limit of 3% for the initial fraction of the $CO_3^-$ anions in the electron radiolysis of sc $CO_2$ is obtained.

To save space, some data and experimental details are given in the Supporting Information. Figures 1S−43S and sections with a designator "S" after the number are placed therein. For a general reader, it is not necessary to consult the Supporting Information every time a reference to this material is given in the main text, because the results obtained therein are briefly summarized and commented upon in the main text. The Supporting Information discusses these data in more detail.

## 2. Experimental Section

The design of high-pressure optical cells used in this study is given in section 1S.3 and Figures 1S−3S. Two cells were used: (i) cell 1 with internal volume of 5 $cm^3$ and optical path of 2.64 cm and (ii) cell 2 with internal volume of 13.4 $cm^3$ and optical path of 5 cm. In cell 1, two stainless steel electrodes separated by 2 mm, with apparent difference 1−5 kV in the potential, are immersed in the solution. The details of the optical and electrical setups are given in section 1S.3 and Figure 4S. The sc $CO_2$ solutions were pressurized and flowed using an HPLC pump; the flow diagrams are given in Figures 5S and 6S, and the operation procedures are discussed in section 1S.3. The pressure was measured with an accuracy of ±50 mbar, and the temperature was controlled to ±0.1 °C. The solvent density and static dielectric constant were calculated using formulas given in the literature.[14] Unless specified otherwise, the data were obtained under the "standard conditions": $\rho = 0.837$ g/$cm^3$ (which corresponds to a solvent pressure of 214 bar and a reduced density of 1.787), $T = 41$ °C ($T/T_c \approx 1.03$), and an external electric field of 25 kV/cm (for the electric field effect experiments). For this density and temperature, the static dielectric constant $\epsilon = 1.513$. Note that our "standard" density is considerably higher than the "standard" density in the studies of Dmitrijevic et al.[1,2] and Takahashi et al.[3] (0.837 vs 0.635 g/$cm^3$). This is due to the difficulty of obtaining rapid, laminar flow of sc $CO_2$ at the low density.

In most of our experiments, the analyzing light from a pulsed Xe arc lamp was coaxial with the electron beam and traveled in the opposite direction. A set of 40 nm fwhm band-pass interference filters was used for wavelength ($\lambda$) selection at 0.33−1 $\mu$m; for 1−2 $\mu$m, a set of 10 nm fwhm band-pass filters was used. The kinetic traces were sampled and averaged at a repetition rate of 0.3 Hz. The typical time sampling interval was 0.2 ns per point. To obtain long-term kinetics (100 $\mu$s to 4 s), cw light from the same Xe arc lamp was used. Cerenkov light and radiation-induced transient absorbance from the cell windows (Figure 13S) were subtracted from the kinetic traces (sections 1S.2 and 1S.3), giving $\Delta OD_\lambda$ vs the delay time $t$. Short 20 MeV electron pulses from the Argonne linac were used for radiolysis (Figure 11S(a)). If not specified otherwise, 7.6 ns fwhm pulses of 65−85 nC were used (trace ii in Figure 11S-(a)), and the repetition rate of the pulses was 0.3 Hz. The *average* doses absorbed by the sample in cells 1 and 2 were 0.81 and 0.88 Gy/nC, respectively. This dose was determined using an aqueous thiocyanate dosimeter (section 1S.2 and Figure 10S);[15] the distribution of the absorbed energy across the cell was determined as described in section 1S.2 (Figures 7S−9S). The time dependence of the dose deposition was obtained by integration of the Cerenkov light signal.

For the field effect experiments (cell 1), the solution was flowed; for scavenging experiments (cell 2), the solution was static. In the latter experiments, the cell was refilled after the exposure to 5−10 electron pulses. Accumulation of radiolytic products rapidly shortens the lifetime of the solvent hole (section 1S.3 and Figure 16S), so that rapid removal of these products is important in the flow experiments. The "natural" lifetime of the solvent hole is further limited to 150−160 ns because of the presence of scavenging impurity in sc $CO_2$ that we used (research grade, Scott Specialty Gases). This impurity is most likely to be water (section 1S.3). The lifetime of the solvent holes varies from one batch of $CO_2$ to another; for "bad" batches, this lifetime is as short as 30−50 ns.

The field-dependent kinetic traces were obtained by averaging 50−200 kinetics with ($\Delta OD_{on}$) and without ($\Delta OD_{off}$) the electric field for a *flowing* sc $CO_2$ solution (the typical flow rate was 2 $cm^3$/min). The field was turned on and off several times during the acquisition. The time-dependent electric field effect $\chi(t)$ on the solvent radical cation yield (observed for $\lambda > 900$ nm) was defined as

$$\chi(t) = \{\Delta OD_{on}(t) - \Delta OD_{off}(t)\}/\Delta OD_{off}(t) \qquad (1)$$

If not specified otherwise, the end-of-pulse field effect $\chi_0$ at the maximum of $\Delta OD_{off}$ ($\lambda = 900$ nm) is given. For $\lambda < 900$ nm, only the difference kinetics, $\Delta\Delta OD = \Delta OD_{on} - \Delta OD_{off}$, are given because several species contribute to the transient absorbance.

## 3. Results

In this section, transient absorbance ($\Delta OD_\lambda$) kinetics in pulse radiolysis of sc $CO_2$, with and without the external electric field, are examined. Basic features of these kinetics are established (section 3.1), and transient optical spectra are decomposed into spectral contributions from several light-absorbing species (section 3.1). A qualitative picture of the electric field effect in sc $CO_2$ is presented, and the dynamics of the electric field effect observed in radiolysis of neat sc $CO_2$ and $SF_6$ and $H_2$ solutions are analyzed (section 3.2). This analysis is continued in section 4.1, using the theoretical models given in the Appendix (sections 2S.2 and 2S.3). The yield of solvent cation as a function of radiolytic dose is studied (section 3.3), and the implications of these dose dependencies for the mechanism of radiolysis of sc $CO_2$ are discussed (section 4.1). Experiments in which the solvent radical cation and/or anion are scavenged using $N_2O$, $O_2$, and CO are examined, and the formation of multimer solute ions is demonstrated spectroscopically (section 3S). Long-term decay kinetics for a neutral product (associated with singlet $CO_3$ in section 4.3) are obtained, and its chemical reactions with several solutes are studied (section 3.4).

**3.1. Transient Absorption Kinetics: Basic Features.** *Long-Lived Light-Absorbing Product.* Save for a wider observation window (1 $\mu$s to 5 s, Figure 1), the kinetics obtained in this study were similar to the decay kinetics reported by Dimitrijevic et al.[1,2] and Takahashi et al.[3] In their studies, the kinetics were followed over the first 200 ns only. Our results indicate that the transient absorbance with an onset at 850 nm and a peak at 550 nm (Figure 1) observed by Takahashi et al. at the delay times >100 ns[3] and attributed by these authors to the solvent radical anion was actually from a long-lived neutral product. The absorbance from this product is observed within the first 100 $\mu$s after the electron beam pulse (Figure 1); at later delay times, it decays over hundreds of milliseconds (Figure 1 and Figures 35S−37S in section 3.4). No spectral evolution is observed for this absorption band in the first 300 $\mu$s after the pulse. At later times, the spectrum changes, and a new absorption band in the red emerges (Figures 35S, 37Sa, and 38Sb in section 3.4). Scavenging experiments suggest that more than one species contribute to the spectrum observed on the submillisecond time scale (see section 3.4 for more detail). The same long-lived absorbance was observed in experiments where the electron and light beams were crossed at the 90° angle (Figure 14S); this detection scheme excludes the possibility that this long-lived absorption is an artifact of the window absorbance subtraction.

The exceedingly long lifetime of the absorbing species (>300 ms) suggests that this species is not an ion, as the ion

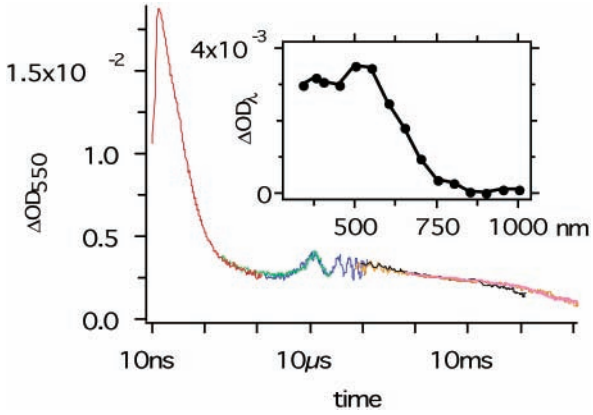


**Figure 1.** Decay kinetics of the $\lambda = 550$ nm absorbance (10 ns to 2.5 s) observed in pulse radiolysis of neat sc $CO_2$ under our standard conditions ($T = 41$ °C and $\rho = 0.837$ g/$cm^3$). The flowing sample (6 $cm^3$/min) in cell 2 was irradiated using 7.6 ns fwhm, 67 Gy pulses from a 20 MeV linac. These kinetics are obtained using collinear electron and light beams and spliced from several runs obtained using a pulsed Xe arc lamp ($t < 100$ $\mu$s, 250 MHz filter, 50 Ω load) or cw light from the same lamp ($t > 100$ $\mu$s, 2 MHz filter, 1 kΩ load; see section 1S.3 for more detail). The "ripple" in the 10−100 $\mu$s time interval is due to instability in the arc. The long-term kinetics are also shown separately in Figure 36S. The insert demonstrates the optical spectrum of the stable light-absorbing product. This spectrum was obtained by integration of the transient absorbance kinetics in the 0.5−1 $\mu$s time window.

recombination is complete in less than 1 $\mu$s (see below). For $t < 1$ $\mu$s, the yield of the long-lived absorbance (unlike that of the solvent radical anion and the solvent radical cation) does not change in the presence of the electric field. No loss of this long-lived species on the millisecond time scale because of discharge at the electrodes was observed in the electric field.[16] All of these observations (and the experiments discussed in sections 3.4 and 3S) suggest that the long-lived 550 nm band is from a stable *neutral* product. This product is formed gradually, over several tens of nanoseconds (see below); there is no prompt formation during the radiolytic pulse (sections 3.2 and 3S). Therefore, this product contribute little to the short-time absorption spectra discussed below.

*Decomposition of the Prompt Spectra.* The typical kinetics obtained in pulse radiolysis of neat sc $CO_2$ is shown in Figure 2, and the evolution of the optical spectra as a function of the observation window is shown in Figure 3. At short delay times, the spectrum is dominated by a bell-shaped band centered at 750 nm. The same band was observed by Dimitrijevic et al.[1,2] and Takahashi et al.[3] and ascribed to the absorbance of the solvent radical cation. In addition to this 750 nm band, there also appears to be a shoulder at 400−500 nm. The time profiles for all decay kinetics observed at $\lambda > 850$ nm are identical. Thus, the absorption spectrum in the red is dominated by a single species: the solvent radical cation. In the previous studies by Dimitrijevic et al.,[1,2] the decay kinetics of the solvent radical cation were obtained at $\lambda = 700$ nm, where several species, including the neutral product, absorb the light. Consequently, their kinetic data were compromised, and rate constant measurements were repeated in this work (Table 1 and Figures 23S and 28S−30S). In these measurements, the decay kinetics of the solvent radical cation were obtained at 900−1000 nm, where no other species absorb.

The composite nature of the prompt spectra shown in Figure 3 becomes apparent when electron or hole scavengers are added to the solution. Addition of $SF_6$ increases the yield of the solvent radical cation severalfold (Figure 4),[1] as this solute rapidly

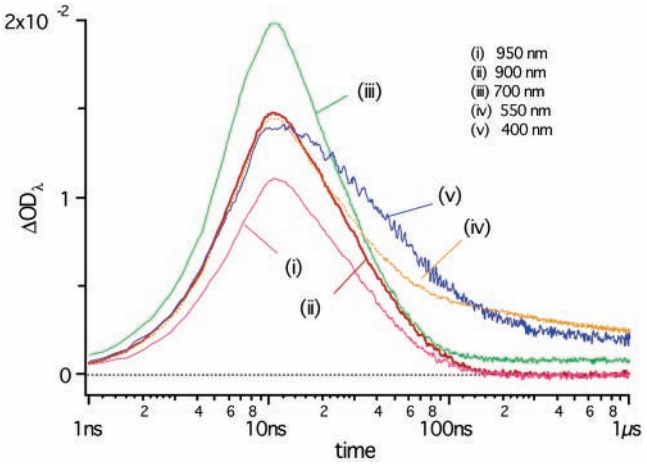


**Figure 2.** Examples of the transient kinetics in pulse radiolysis of neat sc $CO_2$ (same conditions as in Figure 1). The kinetics were obtained at (i) 950, (ii) 900, (iii) 700, (iv) 550, and (v) 400 nm from the same flowing sample. The wavelength ($\lambda$) selection was obtained using a set of 40 nm fwhm interference filters. All kinetics for $\lambda > 850$ nm exhibit the same time profile. The kinetics for $\lambda < 850$ nm exhibit a plateau for $t > 200$ ns because of the formation of the stable product (Figure 1). Note that the decay kinetics in the blue are considerably longer than the kinetics in the red.

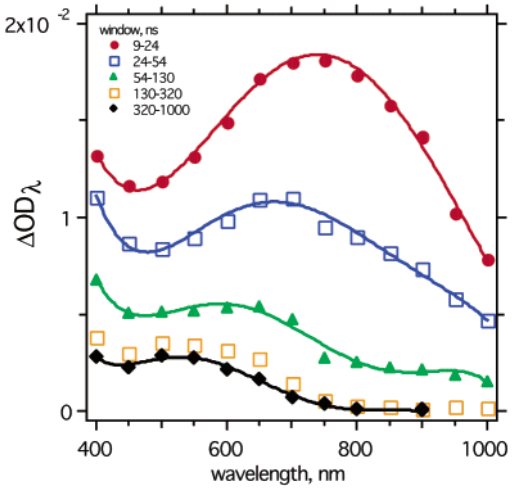


**Figure 3.** Progression of transient absorption spectra obtained in pulse radiolysis of neat sc $CO_2$ (same conditions as in Figures 1 and 2). The time integration windows are indicated in the figure. The prompt spectra (9−24 ns window, filled circles) are dominated by the bell-shaped absorbance band of the solvent radical cation that is centered at 750 nm. Also, in the 400−500 nm, a shoulder from the bound-to-continuum transition of the solvent radical anion is observed. At later delay times (20−200 ns), this shoulder increases relative to the bell-shaped signal because of slower decay of the solvent radical anion relative to the solvent radical cation. On the same time scale, the 550 nm band of the stable product emerges (filled diamonds). This product dominates the spectra obtained for $t > 300$ ns. Solid lines drawn through the symbols are polynominal fits.

scavenges quasifree electrons, by dissociative attachment. The resulting $F^-$ anion has low mobility[4] and recombines with the solvent hole slowly (on the time scale of tens of nanoseconds). Consequently, addition of $SF_6$ dramatically increases the yield of the solvent holes observed on the nanosecond time scale. For example, addition of 7 mM of $SF_6$ increases the maximum $\Delta OD_{900}$ from $1.5 \times 10^{-2}$ to $5.8 \times 10^{-2}$ (Figure 4a) This increase can be simulated theoretically, using the equations given in section 2S.2 (Figure 4b). From the photoconductivity experiments of Shkrob and Sauer,[4] it is known that the solvent radical anion reacts with $SF_6$ with a rate constant of $2.15 \times 10^{10}$ $M^{-1}$ $s^{-1}$. Thus, for $[SF_6] = 0.17$ M, the lifetime of the solvent radical anion is <0.3 ns; this lifetime is considerably shorter than the duration of the 7.6 ns fwhm pulse. Furthermore, at this concentration of $SF_6$, the solute reacts with $e_{qf}^-$ faster than the electron trapping by the solvent occurs;[4] that is, the yield of the solvent radical anions is very low. Consequently, these anions cannot be observed in the concentrated $SF_6$ solutions.

**TABLE 1: Rate Constants for Electron/Proton Transfer to the Solvent Hole in sc $CO_2$ ($T = 41$ °C, $\rho/\rho_c = 1.79$)**

| solute | $IP_{gas}$,[a] eV | rate constant, $M^{-1}$ $s^{-1}$ |
|---|---|---|
| $H_2$ | 15.43 | $(8.1 \pm 0.5) \times 10^{7}$ [c] |
| $O_2$ | 12.07 | $(3.88 \pm 0.2) \times 10^{10}$ [d] |
| $N_2O$ | 12.84 | $(3.95 \pm 0.4) \times 10^{10}$ [d] |
| CO | 14.01 | $(1.26 \pm 0.04) \times 10^{10}$ [d] |
| $n$-$C_{16}H_{34}$ | < 9.56[b] | $\sim 10^{11}$ |

[a] The gas-phase ionization potential for the monomer molecules; the ionization potential for $CO_2$ is 13.77 eV (ref 53). [b] $IP_{gas}$ for $n$-undecane. [c] Proton transfer. [d] Electron transfer.

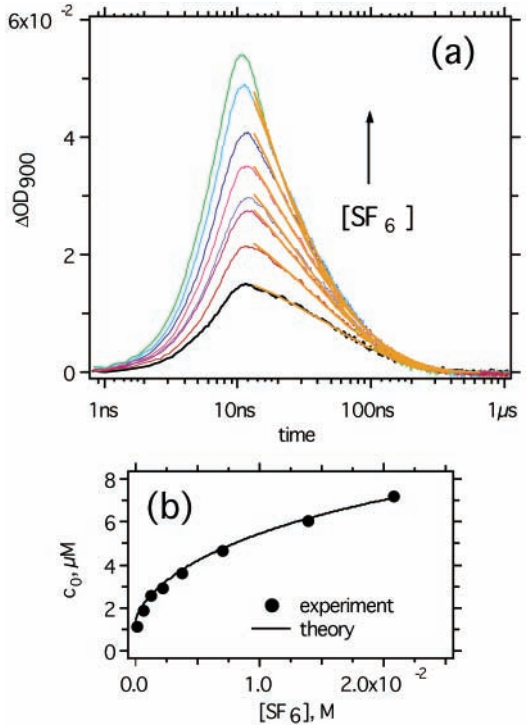


**Figure 4.** (a) Progression of transient absorbance kinetics obtained at $\lambda = 900$ nm from the $SF_6$ solutions in sc $CO_2$. The $SF_6$ concentrations are (from bottom to top): 0, 0.48, 1.16, 2.1, 3.58, 6.9, 13.8, and 20.7 mM. At 900 nm, the absorption is from the solvent radical cation. Bold lines drawn through the kinetics are the multi-trace least-squares fit using eq 3 with parameters given in section 3.1. (b) Initial concentrations $c_0$ of the solvent radical cation plotted vs $[SF_6]$. The solid line is a theoretical curve obtained using the Monte Carlo model discussed in section 2S.2 (see also section 4.1).

Figure 5 shows the prompt absorption spectra for neat sc $CO_2$ and the 0.17 M $SF_6$ solution. These spectra were obtained by integration of the $\Delta OD_\lambda$ kinetics in the 7−25 ns window and normalized at $\lambda = 750$ nm. It is seen from Figure 5 that the two spectra coincide in the 650−1000 nm region and diverge in the 400−650 nm region. Because the prompt spectrum from the $SF_6$ solution (trace ii, Figure 5) is dominated by the absorption of the solvent radical cation, it follows that the 400−500 nm shoulder seen in the spectrum from neat sc $CO_2$ (trace i, Figure 5) should be from a different species whose yield is reduced in the presence of $SF_6$. The subtraction of trace ii from trace i in Figure 5 yields the spectrum of this "missing" species

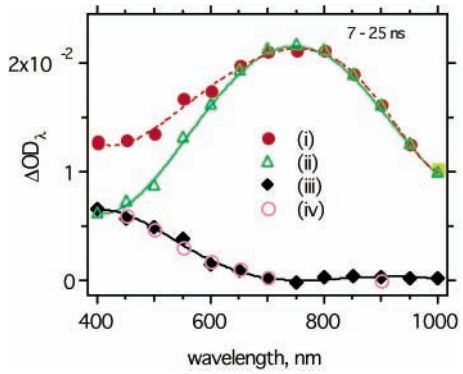


**Figure 5.** Prompt transient optical spectra (7−25 ns window) obtained in radiolysis of (i) neat sc $CO_2$ (filled circles) and (ii) 0.17 M solution of $SF_6$ in sc $CO_2$ (open triangles). Trace ii was scaled down 3.6 times to match the 900 nm absorbance in trace i. Trace iii (filled diamonds) is the difference between traces i and ii. Trace iv (open circles) is the prompt absorption spectrum observed in the 2.87 M solution of $H_2$ in sc $CO_2$.

(trace iii, Figure 5). In the following, it will be demonstrated that this species is the solvent radical anion in sc $CO_2$. Remarkably, a very similar spectrum (trace iv in Figure 5) was obtained in a *hole* scavenging experiment described below.

Takahashi et al.[3] showed that $H_2$ reacts with the solvent radical cation in sc $CO_2$, probably by proton transfer:

$$(CO_2)_n^+ + H_2 \rightarrow H + OCOH^+ + (n-1)CO_2 \qquad (2)$$

Our kinetic measurement (Figure 23S) at $\lambda = 900$ nm gives a rate constant of $(8.1 \pm 0.5) \times 10^7$ $M^{-1}$ $s^{-1}$ for this reaction (for other wavelengths, the kinetics are given in Figures 24S−26S). As more $H_2$ added to the solution, the lifetime of the solvent hole is reduced (Figures 23S and 25S) and the presence of other light-absorbing species becomes apparent (Figures 25S and 26S). When 1.66 M of hydrogen is added, the lifetime of the solvent hole is reduced to 7.4 ns, which is comparable to the duration of the electron pulse. As shown in Figures 25S and 26S, the $\Delta OD_\lambda$ kinetics observed in this 1.66 M $H_2$ solution are weighted sums of two contributions: (i) a signal from a long-lived species (most clearly seen in the red) whose concentration gradually increases with time over 300 ns and (ii) a signal from a short-lived species (most clearly seen in the blue) that decays over the same period of time (Figure 26S). The former signal is from the stable light-absorbing product, Figure 1. Exactly the same generation kinetics for species i were observed in the $O_2$ solutions (Figure 27S and section 3S), over a wider spectral range, and the transient absorbance spectra obtained within the time period of generation (<300 ns) match the spectra of the stable product acquired on the microsecond time scale (Figure 41S(b)). The decaying signal ii is from the solvent radical anion, as shown below.

Figure 6a shows a comparison between the prompt spectra (7−21 ns window) obtained in neat sc $CO_2$ (trace i) and the 1.66 M $H_2$ solution (trace ii). The same absorbance that is increased by addition of $SF_6$ (because of higher yield of free solvent holes) is removed by addition of $H_2$ (because of rapid elimination of the solvent holes by reaction 2). This point is demonstrated by subtraction of trace ii from trace i (Figure 6a) and comparing the difference trace iii to the normalized trace ii in Figure 5 (trace iv in Figure 6a). The residual absorbance (trace ii, Figure 5) has the same spectrum as the difference trace iii in Figure 6a; that is, the species eliminated by addition of $SF_6$ does not react with $H_2$. The difference between the kinetics obtained in neat sc $CO_2$ and the 1.66 M $H_2$ solution yields the

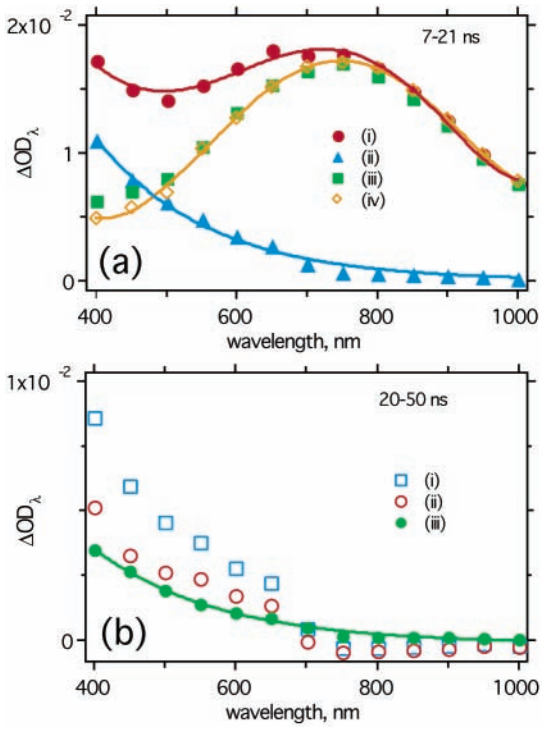


**Figure 6.** (a) Prompt transient optical spectra (7−21 ns window) obtained in radiolysis of (i) neat sc $CO_2$ (filled circles) and (ii) 1.66 M solution of $H_2$ in sc $CO_2$ (filled triangles). Trace iii is the difference of traces i and ii. Compare this difference trace with trace iv which a scaled trace ii in Figure 5a. See Figures 24S to 27S for the kinetics and later-delay spectra in the $H_2$ solution. Addition of hydrogen selectively "removes" the 750 nm band of the solvent radical cation from the absorbance spectra. (b) Transient absorbance spectra obtained in the 20−50 ns window from a 1.66 M solution of $H_2$ in sc $CO_2$ (ii) with and (i) without 25 mM $O_2$ (open circles and squares, respectively). Trace iii (filled circles) is the difference of traces i and ii. Oxygen selectively "removes" the signal of the blue-absorbing solvent radical cation. The difference signal, trace iii, has the same shape as the prompt signal in the $H_2$ solution, trace iii in Figure 6a, and the difference trace iii in Figure 5a, in the $SF_6$ solution.

decay kinetics of the species scavenged by $H_2$ (Figure 24S). Unlike the $\Delta OD_\lambda$ kinetics shown in Figure 2, the time profiles of these difference kinetics do not change with wavelength (450−900 nm), as all of these are the decay kinetics of the solvent radical cation. These spectral and kinetic data prove that addition of $H_2$ selectively "removes" the signal of the solvent radical cation from the transient absorption spectra.

When electron acceptors, such as $O_2$ or $SF_6$, are added to the 1.66 M $H_2$ solution, the blue-absorbing species is scavenged (Figure 5, trace iii, and Figure 6b). This behavior is consistent with the radical anion being the species responsible for the decaying absorbance at $\lambda < 750$ nm. Because addition of oxygen does not change the yield of the stable light-absorbing product (section 3S and Figure 40S therein), the subtraction of the spectra obtained in the 1.66 M $H_2$ solution (trace i in Figure 6b) and the hydrogen solution with $O_2$ added (trace ii in Figure 6b) yields the spectrum of the radical anion that is free from the interference from the product absorbance. Indeed, the residual prompt spectrum (trace ii in Figure 6a) obtained at 7−21 ns (when the product yield is small) is the same as the difference trace iii (Figure 6b) obtained at 20−50 ns, when the product yield is substantial.

Figure 7 demonstrates a comparison between the absorption spectrum of the blue-absorbing radical anion (scaled trace iii in Figure 6b) and the electron photodetachment spectrum of

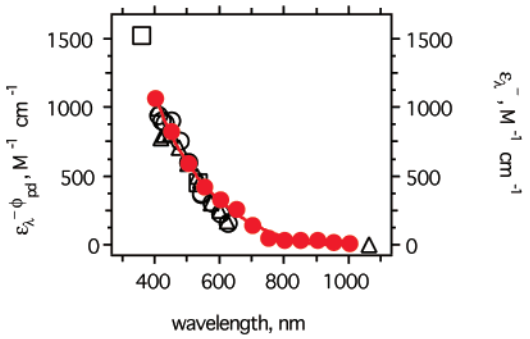


**Figure 7.** Comparison between the electron photodetachment spectrum of the solvent radical anion obtained in the time-resolved conductivity experiment of Shkrob and Sauer (ref 4; open symbols) and the spectrum of the blue-absorbing radical anion generated in pulse radiolysis of sc $CO_2$ (filled circles). The latter is a scaled trace iii in Figure 6b. The extinction coefficients of the radical anion $\epsilon^-_\lambda$ were estimated by comparison of traces i and iii in Figure 5a using the known $\epsilon^+_\lambda$ for the solvent radical cation and assuming the same yield of the solvent radical cation and the radical anion (see section 4.2). The cross section of photodetachment is given as a product of the extinction coefficient and quantum yield $\phi_{pd}$ of the photodetachment.

the solvent radical anion obtained by Shkrob and Sauer.[4] These two spectra are virtually identical. We therefore conclude that the 400−500 nm shoulder observed in the prompt spectra from neat sc $CO_2$ is from the bound-to-continuum band of the solvent radical anion. Further evidence in support of this species is given in section 3.2, where the electric field dependence on the kinetics is examined.

*Decay Kinetics of the Solvent Hole.* The decay kinetics of the solvent radical cation can be observed, without interference from other species, for $\lambda > 850$ nm. For any dose, the kinetics at $t > 20$ ns can be fit by

$$\Delta OD_\lambda = \epsilon^+_\lambda L c_0 \exp(-k_1 t)/(1 + k_2 c_0 t) \qquad (3)$$

where $\epsilon^+_\lambda$ is the extinction coefficient of the solvent radical cation, $L$ is the optical path of the cell, $c_0$ is the initial cation concentration (extrapolated to $t = 0$), $k_1$ is the inverse "natural" lifetime of the solvent hole, and $k_2$ is the rate constant for ion recombination in the bulk (for example, Figure 8a). These kinetics imply that the solvent hole decays by (i) homogeneous ion recombination and (ii) pseudo-first-order scavenging reaction with impurity to yield a secondary cation that recombines with the anion at the same rate as the solvent radical cation (see the discussion of the impurity in section 1S.3). Experimentally, the "natural" lifetime of the solvent hole ($t_h = k_1^{-1}$) varies from one batch of $CO_2$ to another; even for "good" batches, $t_h <$ 160 ns. Unless the solution is rapidly flowed through the cell, this lifetime is further shortened because radiolytic products, such as CO and $O_2$, that accumulate in the solution react with the solvent hole (Table 1, section 1S.3, and Figure 16S therein). On the other hand, complete removal of these products is difficult to achieve practically because using low repetition rates makes the acquisition time exceedingly long whereas using flow rates greater than 6 $cm^3$/min introduces turbulence and light scattering.

Dimitrijevic et al.[1,2] and Takahashi et al.[3] assumed that the decay kinetics of the solvent radical cation are nearly exponential. This is indeed the case when the solution is contaminated by radiolytic products (section 1S.3) because scavenging reaction with these products is faster than ion recombination in the bulk. When these radiolytic products are removed by flowing the

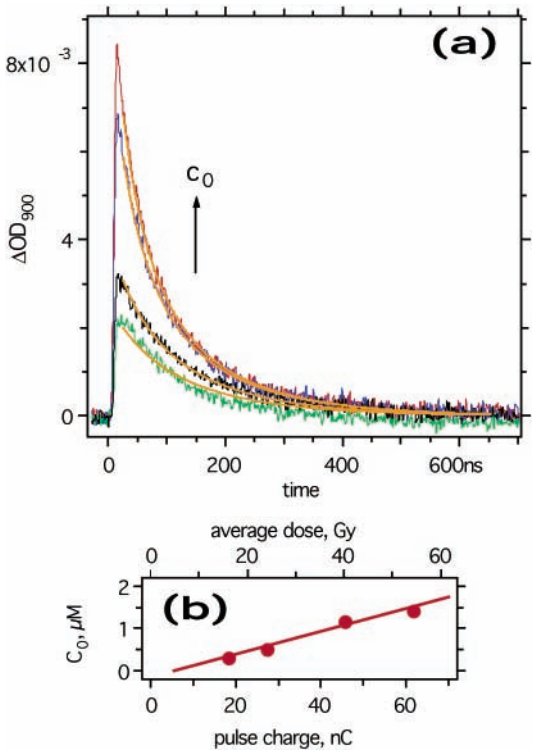


**Figure 8.** Transient absorbance kinetics at 900 nm for 7.6 ns fwhm pulses with charges of 18, 27, 45.5, and 61.5 nC (nano-Coulombs). The solution flowed at 6 $cm^3$/min through cell 1 (volume of 5 $cm^3$), and the repetition rate of the electron pulses was 0.05 Hz. Despite the efficient removal of radiolytic products, the lifetime of the solvent radical cation is ca. 160 ns. This lifetime becomes progressively shorter at higher doses. Bold lines drawn through the kinetics are multitrace least-squares fit obtained using eq 3 with parameters given in section 3.1. (b) Charge and dose dependence of the initial concentration $c_0$ of the solvent radical anions (obtained from the fit shown above).

sample, it becomes evident that for higher doses the decay is faster (Figure 8a). The same shortening is observed in $SF_6$ solutions (Figure 4a). As explained above, addition of the electron scavenger increases the prompt cation yield. This increase has the same effect as changing this yield by increasing the dose. Figure 4a shows the least squares multitrace fit of the $\Delta OD_{900}$ kinetics obtained for several concentrations of $SF_6$. In this simulation, $\epsilon^+_{900}$, $k_1$, and $k_2$ were the same for all kinetic traces; only the initial cation concentration $c_0$ was varied. The recombination constant $k_2$ was approximated by the Debye formula, $k_2 = 1.1 \times 10^{15}\ \mu_i/\epsilon$, where $\mu_i$ is the sum of ion mobilities (in $cm^2$/Vs) and $k_2$ is in $M^{-1}\ s^{-1}$. Using $\mu_i \approx 0.016$ $cm^2$/Vs, one obtains $k_2 \approx 1.17 \times 10^{10}\ M^{-1}\ s^{-1}$. The entire set of these kinetics was simulated using $k_1 = 10^7\ s^{-1}$, $\epsilon^+_{900} \approx$ 3270 $M^{-1}\ cm^{-1}$ and $c_0$ plotted in Figure 4b. Note that the estimate for $\epsilon^+_{900}$ depends on the value assumed for the recombination constant. The solid line drawn through the experimental points for $c_0$ in Figure 4b is the theoretical curve obtained in sections 4.1 and 2S.2.

For neat sc $CO_2$ irradiated using 27−62 nC, 7.6 ns fwhm pulses (cell 1), a multitrace fit obtained in a fashion similar to Figure 4a yields $k_1 = 6.37 \times 10^6\ s^{-1}$ and $\epsilon^+_{900} \approx 3{,}000\ M^{-1}\ cm^{-1}$; the initial cation concentrations $c_0$ are linear with the beam charge (Figure 8b). From these simulations, it appears that the cation yield in neat sc $CO_2$ is ~1 $\mu$M (for a typical 60−70 Gy pulse). Importantly, these simulations suggest that the solvent radical cations generated in radiolysis of neat sc $CO_2$ recombine in bulk; that is, their geminate dynamics are short. The

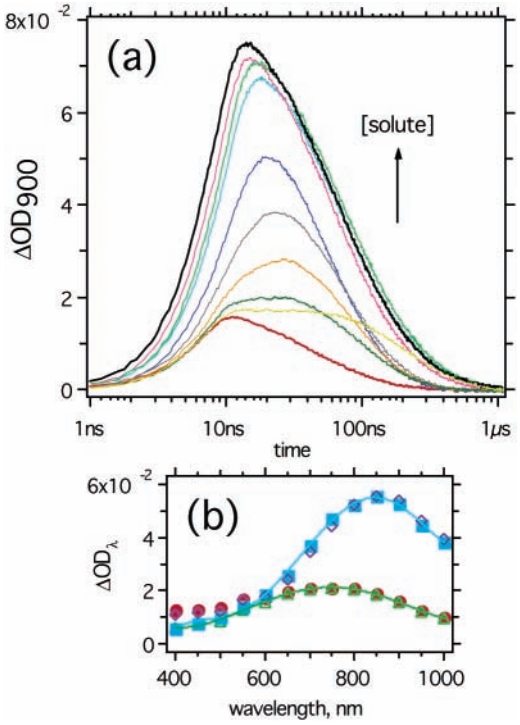


**Figure 9.** (a) Transient absorbance kinetics at 900 nm observed in sc $CO_2$ containing (from top to bottom) 10.2, 7.6, 5.1, 2.5,1.3, 0,8, 0.4, 0.2, 0.1, and 0 mM of *n*-hexadecane. (b) Prompt transient optical spectra (same window) observed (ii) with (open diamonds and filled squares) and (i) without (open triangles and filled circles) 5.2 mM of *n*-hexadecane in sc $CO_2$. Open symbols are from the *n*-hexadecane solutions that contained 0.17 M $SF_6$; these traces were scaled down by 3.6 times to match the spectra obtained in the absence of the electron scavenger. The 900 nm band is from *n*-hexadecane$^+$.

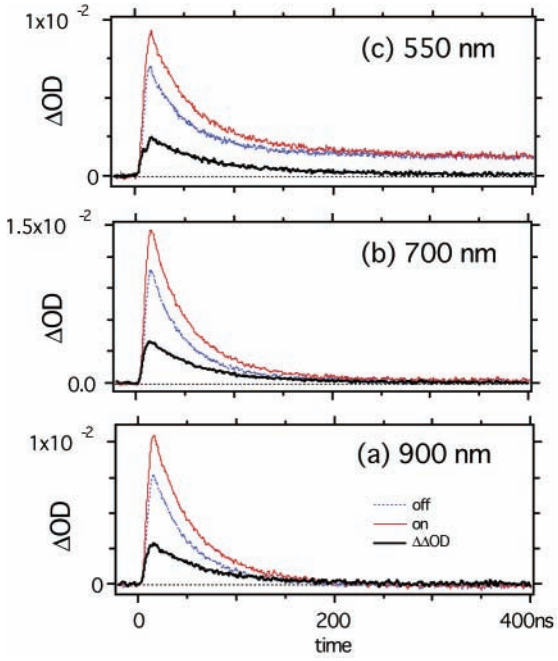


**Figure 10.** $\Delta OD_{off}$, $\Delta OD_{on}$, and $\Delta\Delta OD$ kinetics (section 3.2) obtained at (a) 900, (b) 700, and (c) 550 nm in pulse radiolysis of neat sc $CO_2$. The field-off traces are dashed lines, field-on traces are solid thin lines, and the difference traces are solid bold lines. $\Delta\Delta OD$ kinetics observed at other wavelengths are shown in Figures 31S and 32Sa. The electric field was 25 kV/cm.

conductivity studies of Shkrob and Sauer[4] also suggested that the charge separation in dense sc $CO_2$ ($\rho/\rho_c > 1.2$) occurs predominantly in the electron−hole pairs, in less than 200 ps.

Addition of hole scavengers shortens the 900−1500 nm kinetics. Table 1 gives bimolecular rate constants for $O_2$, CO, $N_2O$, and $H_2$ under our standard conditions. These rate constants were obtained from the plots of $k_1$ vs solute concentration. For $O_2$, $H_2$, and CO, the solute cations ($CO_4^+$, $OCOH^+$, and $(CO)_n^+$) do not absorb at 900 nm, the concentration plots are linear, and the extraction of $k_1$ using eq 3 is straightforward. For $N_2O$, the solute cation rapidly dimerizes to yield the $(N_2O)_2^+$ cation which absorbs at 900 nm (section 3S and Figure 39S therein). For this solute, biexponential fits were used to extract the scavenging rate.

The $\Delta OD_\lambda$ kinetics obtained in the 400−700 nm region are notably slower than the kinetics observed at 900−1500 nm.[3] This is not surprising, as both solvent radical ions and the neutral product contribute to the absorbance at 400−700 nm. As shown in section 3.2, the decay kinetics of the solvent radical anion are slower than the kinetics of the solvent radical cation, as the former species does not react with the impurity that scavenges the solvent hole.

*Extinction Coefficient for the Solvent Radical Cation.* The extinction coefficient $\epsilon^+_\lambda$ of the solvent radical cation was measured by reacting this species with an electron donor, *n*-hexadecane. Typically, such measurements are carried out by reacting the solvent hole with polycyclic aromatic solutes (such as pyrene and perylene) whose radical cations have narrow spectral lines with known extinction coefficients.[17] In this work, *n*-hexadecane was used instead, for the following reasons:

(i) The absorption band of the *n*-$C_{16}H_{34}^+$ is centered in the near-IR, and the spectral overlap with the 750 nm band of the $(CO_2)_n^+$ cation is minimized,[18]

(ii) Aromatic radical cations rapidly dimerize[17] in sc $CO_2$, and the resulting kinetics are complex,

(iii) It is impossible to add more than 0.1 mM of these aromatic compounds to sc $CO_2$ due to their low solubility,

(iv) Unless an electron scavenger (such as $SF_6$) is added, the solvent radical anion also reacts with the aromatic solutes, and the overlapping bands of the solute radical cation and solute radical anion are observed. Addition of $SF_6$ does not simplify the analysis[19] because the $SF_5$ radical (formed in the dissociative electron attachment to $SF_6$) readily oxidizes the aromatic solutes.[17]

Unlike these aromatic solutes, *n*-hexadecane has high solubility in sc $CO_2$ and does not react with $(CO_2)_n^-$ (as shown by our laser conductivity studies)[4] and $SF_5$, and its radical cation does not dimerize.[18] When 5 mM of this solute is added to neat sc $CO_2$ or 0.2 M $SF_6$ solution, a new absorption band centered at 870 nm emerges in the transient absorbance spectra. The ratios $\Delta OD_\lambda/\Delta OD_\lambda^0$ between the prompt spectra obtained with ($\Delta OD_\lambda$) and without ($\Delta OD_\lambda^0$) 5 mM *n*-hexadecane do not depend on the presence of $SF_6$ (compare traces i and ii in Figure 9b). This suggests that the 870 nm band results from a species related to the solvent hole. Its spectrum is very similar to the spectrum obtained in pulse radiolysis of neat *n*-hexadecane;[18] the 800−1000 nm band observed therein is known to be from the corresponding radical cation. For the latter, Mehnert et al.[18] give an extinction coefficient of 9900 $M^{-1}$ $cm^{-1}$ at 900 nm, and we used this estimate for the *n*-$C_{16}H_{34}^+$ cation in sc $CO_2$. Figure 9a shows the progression of the 900 nm kinetics for several concentrations of *n*-hexadecane. At lower concentrations, both the decay kinetics of $(CO_2)_2^+$ and the formation kinetics of *n*-$C_{16}H_{34}^+$ (which has 4.2 times higher extinction coefficient) are observed. For intermediate concentrations, "flattop" kinetics with a maximum that progressively shifts to shorter times for

higher solute concentrations are observed. At higher concentrations, only the formation kinetics of the $n$-$C_{16}H_{34}^+$ cation are observed.

The rate constant of hole scavenging is large, ca. $10^{11}$ $M^{-1}$ $s^{-1}$, which suggests that the main channel for this reaction is charge rather than proton transfer. In neat $CO_2$, the maximum $\Delta OD_{900}$ increases with [*n*-hexadecane] until the latter reaches 2−5 mM; at higher concentration, no further increase is observed. In the $SF_6$ solutions, this saturation does not occur because *n*-hexadecane reacts with the solvent holes in the (relatively) long-lived *geminate* $\{(CO_2)_n^+ F^-\}$ pairs.[20] In neat sc $CO_2$, the lifetime of the primary electron−hole pairs is short, and scavenging of the *geminate* holes is inefficient. From the concentration dependence shown in Figure 9a and the spectra given in Figure 9b, we obtain a decadic molar extinction coefficient of the solvent radical cation at the center of the 750 nm band of 3200 ± 140 $M^{-1}$ $cm^{-1}$, and $\epsilon^+_{900} \approx 2370 \pm 100$ $M^{-1}$ $cm^{-1}$. Note that our estimate of $\epsilon^+_\lambda$ is an upper limit: if proton transfer to *n*-hexadecane occurs as a side reaction, the extinction coefficient is *lower*.

Our estimate for $\epsilon^+_{900}$ is 20% lower than the values extracted from the simulations of the decay kinetics (see above). This does not suggest inconsistency. First, it is possible that our estimate of $k_2$ is too high. Second, the dose distribution in the cell is nonuniform, which causes a spread of the initial cation yields $c_0$ and recombination half-times $(k_2c_0)^{-1}$ across the sample. Because eq 3 is formulated for the *average* cation concentration, the extinction coefficient extracted using this equation could be overestimated. Numerical simulations in which the experimental dose distribution (Figure 7Sb and section 1S.2) and the dose dependence of the cation yield in Figure 19S (section 2S.2) were used showed that the extinction coefficient could be overestimated as much as 15−25%.

Using our estimate for $\epsilon_{750}{}^+$ and the spectra shown in Figure 5, a "composite" spectrum of the solvent radical cation between 5000 to 25 000 $cm^{-1}$ can be obtained (Figure 1 of ref 10). The integration of this spectrum yields an oscillator strength of 0.153. Apparently, the 750 nm band results from a strongly allowed bound-to-bound transition. In ref 10, we argue that this band is from the $X\ ^2B_u \rightarrow A\ ^2A_g$ transition in the $C_{2h}$ symmetric $(CO_2)_2^+$ dimer cation. Following Dimitrijevic et al.,[1,2] we suggest that this dimer cation is the chromophore core of the solvent hole in sc $CO_2$.

**3.2. Electric Field Effect.** *Qualitative Picture.* For the benefit of the reader, a qualitative picture of the electric field effect on the ion yield is given first. It is well-known that a static electric field (1−50 kV/cm) accelerates charge separation dynamics of geminate ion and electron−hole pairs.[21−23] The field pulls the charge carriers apart thereby increasing the free ion yield. For an isolated pair, the increase in the free ion yield FY as a function of the electric field $\mathcal{E}$ is given by Onsager's formula:[21,22]

$$FY/FY_{\mathcal{E}=0} = 1 + \beta_{th} \qquad (4)$$

where $\beta_{th} = e\mathcal{E}r_c/2kT$ and $r_c$ is the Onsager radius, at which the Coulomb attraction $e^2/4\pi\epsilon\epsilon_0 r_c$ between the ions equals their thermal energy, $kT$ ($e$ is the elementary charge and $\epsilon_0$ is the permittivity of vacuum). Note that $\beta_{th}$ does not depend on the initial charge distribution and $FY_{\mathcal{E}=0}$.

Under our standard experimental conditions, $r_c \approx 35.2$ nm and $\beta_{th} \approx 1.62$. The experimental field effect on the prompt yield of the solvent radical cation is 2−4 times lower. As discussed in section 1S.3, this reduction cannot be caused by the loss of the electric field during the electron pulse. Rather, it is a natural consequence of (i) peculiarities of electron dynamics in sc $CO_2$ and (ii) the high-dose regime in which the transient absorbance measurements are carried out. The latter is necessary because of the low sensitivity of the technique to weak chromophores. The conductivity, e.g.,[7,21] and electroluminescence[24] measurements (related to the present technique) use much lower doses and, consequently, are easier to interpret. However, these techniques do not allow for the discrimination between several short-lived intermediates on the basis of their absorption spectra.

Although Onsager's formula gives an upper estimate for the electric field effect on the yield of *free* ions, it does not specify when this effect is attained. The tempo of the charge separation is given in terms of the Onsager time $t_c = r_c^2/D_s$, where $D_s$ is the sum of the diffusion coefficients for geminate partners.[22,23] Numerical simulations indicate that the time-dependent field effect on the ion yield reaches Onsager's value for $t/t_c > 10-100$ (section 2S.2). From the photoconductivity studies of Shkrob and Sauer,[4] it is known that the lifetime-mobility product $\mu_e\tau_e$ of quasifree (conduction band) electrons in dense sc $CO_2$ is $2.5 \times 10^{-9}$ $cm^2/V$. Using Einstein's formula, $D_e = (kT/e)\,\mu_e$ for the diffusion coefficient $D_e$ of the quasifree electron, we obtain for the value of the ratio $\tau_e/t_c$ of the electron trapping time $\tau_e$ and the Onsager time $t_c$ ca. 5.5. In other words, because of rapid trapping of the conduction band electron by the solvent, *the lifetime of the primary electron−hole pair is too short for the electric field effect to develop fully*. The degree of the reduction in the electric field effect is a function of the (known) $\tau_e/t_c$ ratio and the (unknown) distribution of the electron thermalization distances. Monte Carlo calculations in section 2S.2 indicate that, for the thermalization distances ∼10 nm (obtained from the photoconductivity studies), this reduction is ca. 40−60%, in agreement with experiment (see below).

In neat sc $CO_2$, the electron trapping time $\tau_e$ is short (<200 ps)[4] and the electron escape is efficient ($\tau_e/t_c > 1$), so that most of the observed electric field effect develops in the short-lived *primary electron−hole pairs*, well within the duration of the generation pulse. Though there could be an additional, delayed increase in the field effect because of charge separation dynamics in the secondary pairs (of the solvent radical cation and the solvent radical anion), this aftergrowth is slow because the Onsager time of these secondary pairs is long, ca. 30 ns.[4] Thus, most of the solvent radical cations recombine in the bulk before this "secondary" effect takes over. In concentrated $SF_6$ solutions, the lifetime of $e_{qf}^-$ is extremely short and the prompt electric field effect on the cation yield is negligible. Because the mobility of $F^-$ is low,[4] the Onsager time for the $\{F^-(CO_2)_n^+\}$ pair is long (≈78 ns)[4] and the increase in the electric field effect as a function of the delay time is extremely slow. The same applies to the $\{CO_3^-\ (CO_2)_n^+\}$ pairs formed via dissociative electron attachment (see the Introduction).

The qualitative picture discussed above pertains to *isolated* geminate pairs. In our system, the homogeneous recombination of the ions occurs in less than 1 μs. Because the electrons are $>10^3$ more mobile than these ions, cross recombination of the electrons and the holes is important. The "critical" concentration $C_{cr}$ for this electron−hole recombination is given by $C_{cr} = (k_{e-h}t_c)^{-1}$, where $k_{e-h}$ is the corresponding Debye constant ($\sim 4\pi r_c D_s$). Simple calculation shows that $C_{cr}$ is a function of $r_c$ only (section 2S.2). For our system, $C_{cr} \approx 3$ μM, whereas the typical yield of the solvent radical cations in neat sc $CO_2$ is 0.5−2 μM (section 3.1). Consequently, the cross recombination considerably shortens the electron lifetime and reduces the electric field effect. The same applies to the secondary geminate

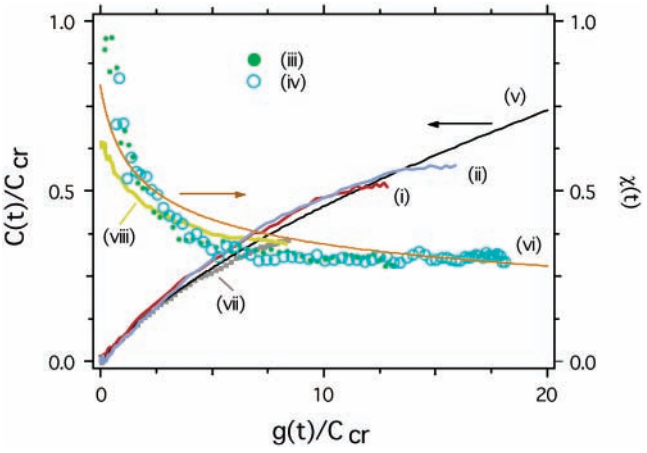


**Figure 11.** Dependence of the yield $c(t)$ of the solvent radical cation (traces i and ii) and the electric field effect $\chi(t)$ (traces iii [filled circles] and iv [open circles]), eq 1, on the total yield $g(t)$ of the electron−hole pairs. The concentrations $c(t)$ and $g(t)$ are given in units of "critical" concentration $C_{cr}$ (sections 3.2 and 2S.2) which, under our standard conditions, is 3.02 $\mu$M. To obtain $g(t)$, the Cerenkov light signal was integrated and scaled using the total average dose (cell 1) obtained using a thiocyanate dosimeter (section 1S.2). The yield of 5 electron−hole pairs per 100 eV was assumed (sections 4.1 and 2S.3). Concentrations $c(t)$ were obtained from the $\Delta OD_{900}$ kinetics assuming the optical path length of 2.64 cm and $\epsilon^{+}_{900} = 2370\ M^{-1}\ cm^{-1}$. Two sets of data are shown. Traces i and iii were obtained using a 7.6 ns fwhm pulse. Traces ii and iv were obtained using a longer (50 ns) pulse (that was similar in shape to trace iii in Figure 11S(a)). Traces v and vi are theoretical results for the cation yield and electric field obtained using the semianalytical treatment of section 2S.2 with the parameters given therein (see also section 4.1). Traces vii and viii are the corresponding to theoretical traces obtained using the lattice Monte Carlo model of section 2S.3.

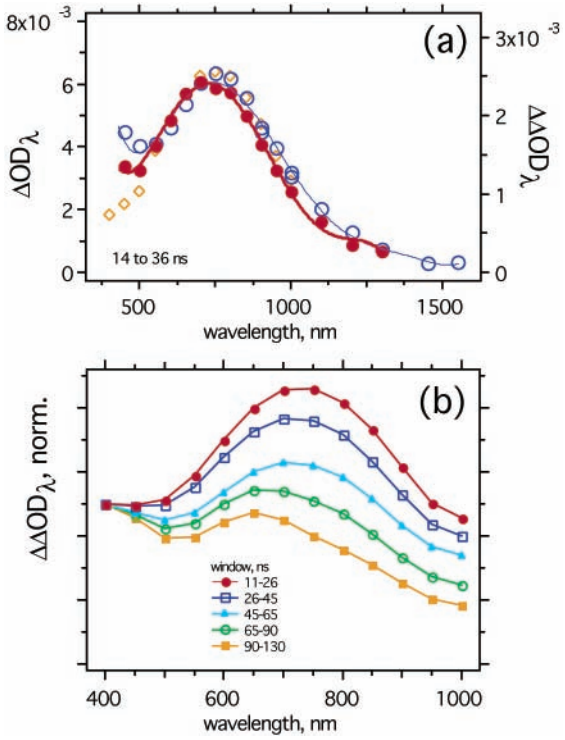


**Figure 12.** (a) Prompt $\Delta OD_{off}$ (open circles) and $\Delta\Delta OD$ (filled circles) spectra (14−36 ns window) obtained in radiolysis of neat $CO_2$. For comparison, a scaled trace ii in Figure 5 is shown by empty diamonds. (b) Time evolution of normalized $\Delta\Delta OD$ spectra. The time integration windows are given in the plot; the spectra were normalized at $\lambda = 400$ nm. The 750 nm band of the solvent radical cation progressively decreases relative to the absorbance band of the solvent radical anion in the blue. The neutral light-absorbing product does not contribute to the $\Delta\Delta OD$ spectra. See also Figure 32S.

pairs, as the efficiency of cross recombination does not depend on charge mobility. From this examination, it follows that the electric field effect decreases with the dose. We refer the reader to section 2S for rigorous examination of this dose effect.

*Electric Field Effect in Neat sc $CO_2$.* Figure 10a exhibits typical $\Delta OD_{on}$, $\Delta OD_{off}$, and $\Delta\Delta OD$ traces observed at $\lambda = 900$ nm. For $t > 30$ ns, these three kinetics are the same: the electric field acts within the duration of the radiolytic pulse. The field effect $\chi_0$ on the cation yield attained by the end of the pulse (where $\Delta OD_{off}$ is maximum) linearly scales with the electric field (Figure 15S(b)), in agreement with eq 4. Note that $\chi_0 \sim 0.3-0.4$, well below the estimate of $\beta_{th} \approx 1.62$ from Onsager's formula. Figure 15S(a) shows the dose dependence of $\chi_0$. To obtain this plot, the pulse duration was fixed and the charge changed as indicated. In agreement with the arguments given above, $\chi_0$ systematically decreases with the dose increasing. In Figure 11, the time-dependent electric field effect $\chi(t)$ (eq 1) observed within the duration of the electron pulse is plotted as a function of the accumulated yield of the electron−hole pairs, $g(t)$. The latter was obtained as specified in sections 3.3 and 1S.2. It is seen that the electric field effect rapidly decreases with $g(t)$, from 0.8 in the beginning of the 7.6 nm fwhm pulse to ≈0.3 by the end of this pulse. Again, such behavior is consistent with the qualitative picture given above.

Figures 10b,c and 31S show the $\Delta OD_{off}$ and $\Delta\Delta OD$ kinetics obtained for $\lambda < 850$ nm. All of these $\Delta\Delta OD$ traces (unlike the $\Delta OD_{off}$ traces) decay to zero in 200−400 ns, regardless of the detection wavelength $\lambda$. Apparently, the yield of long-lived absorbance from the neutral product does not depend on the electric field and this product does not contribute to the $\Delta\Delta OD$ kinetics. In Figure 12, 400−1000 nm spectra obtained by time integration of the $\Delta\Delta OD$ and $\Delta OD_{off}$ kinetics are compared (see also Figure 32S). Shortly after the pulse, the $\Delta\Delta OD$ and $\Delta OD_{off}$ spectra are similar (Figure 12a and Figure 32S). In the blue, both of these spectra are different from the spectrum of the solvent hole shown in trace ii, Figure 5. Apparently, in addition to the solvent radical cation, there is a blue-absorbing ion whose yield is sensitive to the electric field. The corresponding field effect is nearly the same as the effect on the cation yield and develops on the same fast time scale. The latter means that this effect originates through the geminate dynamics of the electron−hole pairs. Only the solvent radical *anion* could be such an ion. Thus, Figure 12a provides conclusive evidence that the blue-absorbing species is the solvent radical anion.

Within the experimental error, the $\Delta\Delta OD$ kinetics obtained at 700−1500 nm (where the solvent radical cation predominantly absorbs) are independent of wavelength, whereas for $\lambda < 550$ nm (where both solvent ions absorb), these decay kinetics become progressively longer at shorter wavelengths (Figure 33S-(a)). A comparison between the 400 and 900 nm $\Delta\Delta OD$ kinetics (Figure 33S(a)) indicates that, in the blue, the half-time of the decay is ≈2 times longer than in the red. Normalized $\Delta\Delta OD$ spectra shown in Figure 12b demonstrate that, at longer delay times, the relative weight of the absorbance from the solvent radical anion increases as compared to the bell-shaped absorbance from the solvent radical cation (see also Figure 32S(b,c)). Both of these trends can be accounted for provided that *the solvent radical anion has longer lifetime as compared to the solvent radical cation*. The half-life for the decay of the $\Delta\Delta OD$ kinetics obtained at 400 nm is close to $(k_2c_0)^{-1}$ estimated using eq 3.

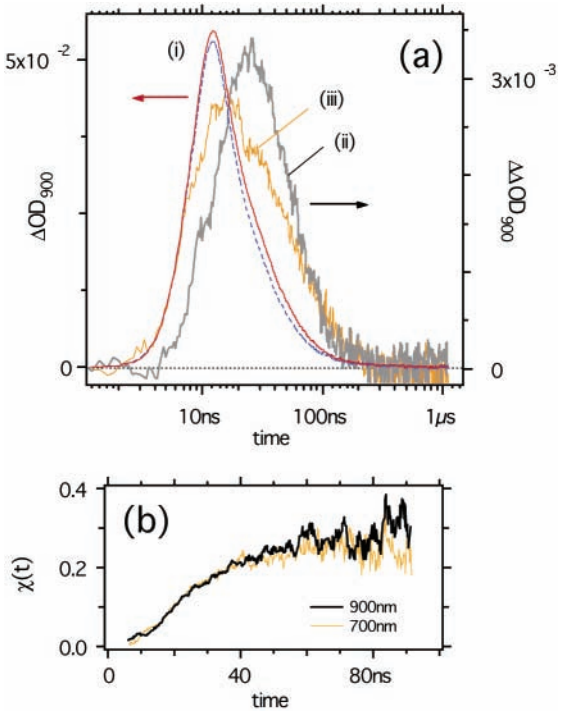


**Figure 13.** (a) $\Delta OD_{off}$ (trace i, dashed line) $\Delta OD_{on}$ (trace i, solid line) and $\Delta\Delta OD$ kinetics (trace ii) obtained at 900 nm from the 0.17 M solution of $SF_6$ in sc $CO_2$. For comparison, $\Delta\Delta OD$ kinetics obtained in neat sc $CO_2$ (under the same irradiation conditions) are shown in trace iii. Unlike the $\Delta\Delta OD$ kinetics in neat sc CO (Figures 31S and 33Sa), time profiles of the $\Delta\Delta OD_\lambda$ kinetics in the $SF_6$ solution do not change with the detection wavelength $\lambda$ (see Figure 33S(b)). (b) Time dependence of the field effect in the $SF_6$ solution. Only 700 and 900 nm kinetics are shown.

*Electric Field Effect in $SF_6$ and $H_2$ Solutions.* Addition of 0.16 M $SF_6$ drastically reduces the lifetime of $e_{qf}^-$ so that only secondary geminate pairs can contribute to the electric effect on the ion yield. Figure 13b confirms this prediction: addition of $SF_6$ fully eliminates the prompt effect on the cation yield. Instead, $\chi(t)$ slowly increases over tens of nanoseconds, reaching $\approx$0.25 at 80 ns. Because of low intensity of the $\Delta OD_{off}$ signal at longer delay times (Figure 13a), we cannot follow the $\chi(t)$ kinetics after 100 ns. As argued earlier, the slow increase in $\chi(t)$ is due slow charge separation dynamics in the secondary geminate pairs. Because this increase is countered by rapid homogeneous recombination of the ions in the bulk, the maximum effect is small.

In this 0.16 M $SF_6$ solution, all $\Delta\Delta OD$ kinetics (unlike the corresponding $\Delta OD_{off}$ kinetics) have the same time profile regardless of the detection wavelength (Figure 33S(b)). This is understandable because the $\Delta\Delta OD$ spectrum is from the solvent hole alone: the blue-absorbing solvent radical anion is not formed in these $SF_6$ solutions, and the neutral product does not contribute to the $\Delta\Delta OD$ kinetics.

The prompt $\Delta OD_{off}$ spectra observed in the 0.1−2 M $H_2$ solutions can be decomposed into the sum of the absorbances from the solvent radical anion and (at lower $H_2$ concentrations) a small residual absorbance from the solvent hole. At longer delay times, the 550 nm band of the neutral product gradually appears (Figures 14 and 26S). For $\lambda < 700$ nm, these formation kinetics are superimposed on the decay kinetics of the solvent radical anion. This anion and its precursor, the electron, can be reacted with $O_2$ (section 3S and ref 4). Figure 14 shows the 550 nm kinetics obtained in 1.75 M $H_2$ solution containing no (trace i) and 25 mM $O_2$ (trace ii). At this $O_2$ concentration, the

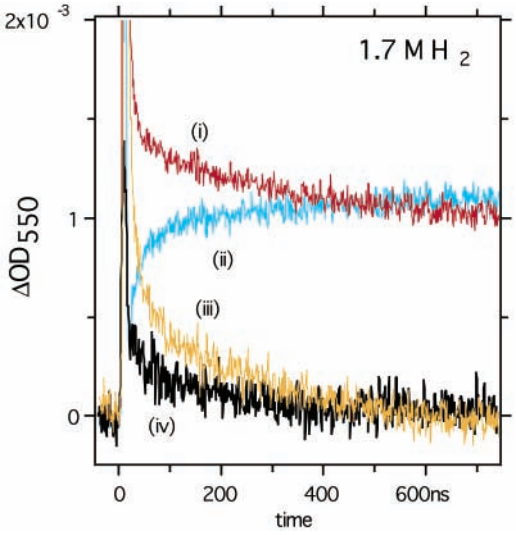


**Figure 14.** Field-off $\Delta OD_{550}$ kinetics obtained in (i) a 1.7 M solution of $H_2$ in sc $CO_2$ and (ii) a hydrogen solution that also contained 23 mM $O_2$. In the latter solution, the absorbance signal is mainly from the neutral product whose gradual accumulation is observed over the first 400 ns after the pulse. The initial "spike" ($t < 20$ ns) is from the solvent radical cation that is rapidly scavenged by $H_2$. Trace iii is the difference of traces i and ii; this trace yields the decay kinetics of the solvent radical anions (the corresponding spectrum is shown in trace iii, Figure 6b). Trace iv is the $\Delta\Delta OD_{550}$ kinetics observed in the 1.7 M $H_2$ solution (with no oxygen added).

electrons and solvent radical anions are converted to $CO_4^-$ within the duration of the electron pulse. At $\lambda = 550$ nm, the absorption of the oxygen ions is small (section 3S), and the signal shown in Figure 14, trace ii, is from the neutral product (the "spike" at $t < 20$ ns is from the solvent hole). Subtraction of the kinetics obtained in the $H_2$ solution with and without $O_2$ yields the decay kinetics of the solvent radical anion (trace iii in Figure 14). That these kinetics are from the solvent radical anion alone can be demonstrated by subtraction of the corresponding spectra (as in Figure 6b): within the first 200 ns, these difference spectra retain the same shape as the $(CO_2)_n^-$ anion shown in Figures 5 and 6.

Because in the 1.75 M $H_2$ solution the lifetime of the solvent radical cation is <8 ns, this cation does not contribute to the $\Delta\Delta OD$ kinetics after the first 30 ns. As the neutral product also does not contribute to $\Delta\Delta OD$, these kinetics are from the solvent radical anion alone. Figure 14 shows $\Delta\Delta OD$ (trace iv) and $\Delta OD_{off}$ kinetics (trace i) obtained in the 1.75 M $H_2$ solution at 550 nm. The apparent field effect is small because most of the $\Delta OD_{off}$ absorbance is from the neutral product. Despite poor signal-to-noise ratio, it is clear that the $\Delta\Delta OD$ kinetics, trace iv, are similar to the difference kinetics, trace iii. Using the latter trace as a reference, the field effect $\chi_0$ on the anion yield is close to the value of 0.4 observed for the field effect on the cation yield. We conclude that the solvent radical anion decays slowly, by recombination in the bulk. By contrast, the solvent hole rapidly decays in a scavenging reaction with impurity.

The result shown in Figure 14 completes our proof that the absorbance in the blue (which is superimposed on the bell-shaped 750 nm absorbance band of the solvent radical cation) is from the *solvent radical anion*. Here, we retrace the steps of this proof: First, it has been shown that electron scavengers, such as $SF_6$, selectively react with the blue-absorbing species. Second, it has been demonstrated that the residual absorbance observed in a solution containing $H_2$ (a hole scavenger) is the same as the absorbance that was removed by addition of these

electron scavengers; that is, the blue-absorbing species is a radical anion. Third, the absorption spectrum of this anion was isolated and compared with the electron photodetachment spectrum of the solvent radical anion obtained in the conductivity experiments of Shkrob and Sauer.[4] The two spectra are virtually the same, which suggests that the blue-absorbing radical anion is the solvent radical anion (rather than $CO_3^-$ and/or an impurity anion). Fourth, it has been shown that the electric field effect on the yield of this anion is formed on the same fast time scale as the field effect on the cation yield. This indicates that both of these effects originate through the geminate dynamics of the primary electron−hole pairs. The only radical anion that can exhibit such prompt electric field effect is the solvent radical anion, as explained above. Fifth, it has been shown that the decay kinetics of the solvent radical anion (because of ion recombination in the solvent bulk) are longer that the decay kinetics of the solvent radical cation (that are mainly due to a reaction with impurity) which accounts for increased weight of the blue-absorbing anion as compared to the red-absorbing cation at longer delay times.

**3.3. Dose Dependence and the *G* Values.** *Qualitative Analysis.* Let us summarize the observations of sections 3.1 and 3.2: Ionization of the solvent results in the formation of short-lived electron−hole pairs. The electric field effect originates through the recombination dynamics of these primary pairs. The electric field acts to increase the separation of the geminate electron, thereby increasing free electron yield. Though quasifree electrons are rapidly trapped by the solvent, most of these electrons escape the Coulomb field of the solvent hole before they are trapped, because of their extremely high mobility. The trapped electrons (solvent radical anions) then slowly recombine with the solvent holes in the bulk; these secondary pairs contribute little to the formation of the electric field effect on the cation yield. Because of scavenging by impurity and radiolytic products, the decay kinetics of the solvent holes are faster than the decay kinetics of the solvent radical anions.

One more way to verify this mechanism is to study the dose dependence of the cation yield. Assume $C = E + I$ is the concentration of the solvent radical cation, $E$ and $I$ are the concentrations of $e_{qf}^-$ and the solvent radical anion, respectively, $k_{e-h}$ is the Debye constant for the electron−hole recombination, and $\tau_e$ is the free electron lifetime (to the first approximation, we assume that the geminate recombination is extremely rapid, $\tau_e/t_c \gg 1$). The generation rate of the primary pairs is given by $G(t)$, and the free electron yield for the primary pair is $\phi_e$. Then, we obtain the following system of kinetic equations

$$dE/dt = \phi_e G(t) - E/\tau_e - k_{e-h}EC \quad (5)$$

$$dI/dt = E/\tau_e \quad (6)$$

(We neglect cross-recombination and scavenging reactions of the ions that occur on much slower time scale). Because $\phi_e\tau_e G(t) \ll 1$, we let $dE/dt \approx 0$, $E \approx C$, and $I \approx C$, to obtain

$$dC/dt = \phi G(t)/(1 + C/C_e) \quad (7)$$

which gives

$$C + 1/2[C^2/C_e] = \phi_e \int_0^t G(t')\, dt' = \phi_e g(t) \quad (8)$$

where $C_e = (k_{e-h}\tau_e)^{-1}$. For $C > C_e$, the second term in eq 8 prevails and $C(t) \propto g(t)^{1/2}$. Thus, *for sufficiently large doses, the cation yield scales as the square root of the time-integrated dose g(t).* Nonuniform distribution of radiolytic dose across the cell does not change this power dependence (section 1S.2).

**TABLE 2: End-of-the-pulse Products $G\epsilon^+_{750}$ of the Radiolytic Yield $G$ of the Solvent Radical Cation (Given in Units of Ions per 100 eV of Absorbed Radiation) and the Decadic Molar Extinction Coefficient $\epsilon^+_{750}$ of the Solvent Radical Cation at 750 nm (Given in Units of dm$^3$ mol$^{-1}$ cm$^{-1}$), in sc $CO_2$ at $T = 41$ °C**

| pulsewidth ns[a] | charge, nC | average dose, Gy[b] | $G\epsilon^+_{750}$ [c] | $G\epsilon^+_{750}$ [d] |
|---|---|---|---|---|
| 4 | 36 | 32.2 | 951 | 1457 |
| 10 | 84 | 67 | 811 | 1223 |
| 20 | 123 | 90.2 | 677 | 1034 |

[a] Nominal pulse width (see Figures 23S and 27S to 30S for actual time profiles of these pulses). [b] Average dose in cell 2, as determined using aqueous thiocyanate dosimeter. [c] $\rho = 0.837$ g/cm$^3$. [d] $\rho = 0.636$ g/cm$^3$.

*Cation Yield vs Dose in Neat sc $CO_2$.* Aqueous thiocyanate was used as a dosimeter to determine the *average* dose absorbed by the sample (section 1S.2). The time profile of $g(t)$ was determined by integration of the Cerenkov light. The *average* cation concentration was obtained from the $\Delta OD_{900}$ kinetics using molar extinction coefficient of 2370 M$^{-1}$ cm$^{-1}$ (section 3.1) and the known optical path (Figure 34S(a)). Typical dose dependencies of the cation yield are shown in Figures 11, 11S-(b), 12S, and 34S(a). Regardless of the cell geometry and the irradiation conditions (beam focusing, length, collimation, etc.), all such dependencies are curvilinear (Figure 12S). The least-squares fit of these plots (Figure 11S(b)) yields $C \propto g^\beta$ with $\beta = 0.607 \pm 0.006$. This exponent is close to $\beta = 1/2$ given by eq 8.

Dimitrijevic et al.[1,2] estimated that for $\rho = 0.635$ g/cm$^3$ and $T = 40.1$ °C, the product $G\epsilon^+_{750}$ of the radiolytic yield $G$ of the solvent radical cation (given in the number of species per 100 eV of absorbed radiation) and the extinction coefficient of the cation at 750 nm was ca. 1300 M$^{-1}$ cm$^{-1}$ (100 eV)$^{-1}$.[25] Because the dose dependence is nonlinear, the $G$ values are dose- and time-dependent. The value reported by Dimitrijevic et al.[1,2] was obtained at the end of a 5 ns fwhm, 27.5 Gy electron pulse. We redetermined this $G\epsilon^+_{750}$, at $\rho = 0.636$ g/cm$^3$ and $\rho = 0.837$ g/cm$^3$, for three pulse durations (Table 2). As seen from Table 2, $G\epsilon^+_{750}$ decreases with the dose, as expected from the plot in Figure 11. Figure 34S(b) shows $G\epsilon^+_{750}$ as a function of the absorbed dose. For a 5−10 Gy dose, this quantity approaches 2000 M$^{-1}$ cm$^{-1}$ (100 eV)$^{-1}$, whereas for a 50−60 Gy dose, $G\epsilon^+_{750}$ is 700 M$^{-1}$ cm$^{-1}$ (100 eV)$^{-1}$. Given these time dynamics, the only way to characterize the radiolytic yield is to simulate the *entire C* vs *g* dependence theoretically and compare it with the experimental dependence. To make such a comparison, one needs to know the radiolytic yield $G_{e-h}$ of the primary electron−hole pairs. This yield was estimated using the kinetics obtained in a concentrated $SF_6$ solution (where the primary pairs have negligible lifetime), by finding $G_{e-h}$ at which both the $\Delta OD_{off}$ and $\chi(t)$ kinetics can be fit simultaneously. We refer the reader to section 2S.3 for details of the simulation procedure. The net result is that there are $5.1 \pm 0.1$ ionization events per 100 eV. Using this estimate, a theoretical curve in Figure 11 was obtained.

Though the experimental and theoretical dose dependencies shown in Figure 11, 11Sb, and 34Sa are similar, the experimental plots varied with the exact procedure used to obtain the data. For example, different dose dependencies were obtained using cell 2 with and without the electron beam collimator (Figure 12S and section 1S.2). These variations were due to (i) nonuniform dose deposition and (ii) light reflection by the cell

walls. The latter can be reduced by better collimation of the electron and light beams (section 1S.2). Calculations in section 1S.2 (Figure 9S(b)) suggest that nonuniform dose deposition results in ca. 12% lower *average* cation concentration for a given *average* dose as compared to the theoretical plot shown in Figure 19S (obtained for an infinitely thin sample). With this correction in mind, we estimate that the cation yield is 10−20% higher than the theoretical values. We will continue the discussion of the dose dependence in section 4.2.

**3.4. Long-Term Kinetics and the Light-Absorbing Neutral Product.** After the first 1 $\mu$s, the solvent ions recombine, and the residual absorbance is from a long-lived product whose absorption band peaks at 550 nm. As pointed out in section 3.2, the initial yield of this light-absorbing product does not depend on the electric field; nor is there an effect of the electric field on the long-term kinetics (<1 s).[16] Apparently, the product is a neutral species. The yield of the 550 nm absorbance is linear with dose, yielding $G\epsilon^{p}_{550} \approx 145 \pm 10$ $M^{-1}$ $cm^{-1}$ (100 eV)$^{-1}$. Neither the spectrum of this product nor the yield of the long-lived absorbance change with the flow rate of the sample and the repetition rate of the electron pulses, suggesting that neither the product nor its precursor react with the radiolytic products accumulated in the radiolysate.

Within the first 100 $\mu$s, the spectra are time independent. However, after the first 1 ms, a small shoulder at 750 nm gradually emerges (Figure 35S(a)). On this millisecond time scale, the $\Delta OD_{550}$ signal slowly decays, decreasing by 20−30% over the first 200 ms (Figure 35S(b), trace i and Figure 36S). Addition of 0.2−0.5 M of $N_2$, $O_2$, and $N_2O$ has no effect on these decay kinetics. By contrast, addition of CO changes the kinetics drastically (Figure 35S(b)): the $\Delta OD_{550}$ signal decays to a new steady level that is 4 times lower than that in neat sc $CO_2$ (this new absorbance was too small to obtain a good-quality spectrum). The rate constant of the corresponding reaction is $770 \pm 30$ $M^{-1}$ $s^{-1}$. Because the reaction with CO is inefficient and reaction with $O_2$ does not occur at all, even prolonged radiolysis has little effect on the kinetics. Addition of hydrogen has same effect as the addition CO, but the reaction is slower (<200 $M^{-1}$ $s^{-1}$).

On a longer time scale, the decay of the 550 nm absorbance lasts over hundreds of milliseconds (Figure 36S); even after 2 s, there is a $\Delta OD_{550}$ signal that is ∼25% of the absorbance at 100 $\mu$s. Though the kinetic traces can be fit by second-order kinetics with a time constant of 330 ms (Figure 36S(b)), in the low-dose regime (20−120 Gy per single pulse), no changes in the kinetics with the pulse dose were observed. Using a 30 Hz burst of 60 Gy pulses causes the accumulation of the product on the observation time scale (Figures 37S and 38S). After 20−30 pulses, the yield saturates (Figure 38S). It is seen from the kinetic plots in Figure 37S(a) that in the high-dose regime the decay kinetics of the product become shorter as the total dose (summed over the sequence of pulses) increases. The spectra obtained on the millisecond time scale using the pulse bursts are composite: in addition to the 550 nm band observed at short delay times, a new 950 nm band emerges, see Figure 38S(b). For $\lambda > 600$ nm, the accumulation kinetics are different from the kinetics observed at $\lambda < 600$ nm (compare traces ii and iii in Figure 38S(a)). The formation of the 700−1000 nm band can also be observed on the submillisecond time scale (Figure 37S(b)). The $\Delta OD_{900}$ kinetics are not complementary to the $\Delta OD_{550}$ kinetics, and the red-absorbing species is unlikely to be related to the 550 nm absorbing product.

## 4. Discussion

**4.1. Quantitative Simulation of the Charge Dynamics.** We have already given a qualitative picture for the ionization dynamics in sc $CO_2$. In this section, we demonstrate that these dynamics can be understood quantitatively, using the set of parameters obtained from the time-resolved conductivity studies.[4] From these studies, it is known that under our standard conditions the ratio of lifetime $\tau_e$ of the electron to the Onsager time $t_c$ of the electron−hole pair is ≈5.5 and the width $b_G$ of the $r^2$-Gaussian distribution of the electron thermalization distances is ≈10 nm. For this distribution, the free ion yield is ≈5.6%.

In section 2S, the model of Shkrob and Sauer[4] is adapted for the present experiment. It is shown that for an isolated ion pair, the electric field effect on the yield of free cations is a function of two paraneters: the $\tau_e/t_c$ ratio and the width $b_G$ of the electron thermalization distances. In Figure 18S(a), this electric field effect (for 25 kV/cm) is plotted as a function of $\eta = \tau_e/t_c$ for several values of $b_G$. For a fixed $\tau_e/t_c$, the effect systematically decreases with $b_G$. The observed initial field effect on the yield of the solvent hole is $\approx 0.8 \pm 0.05$. For $\tau_e/t_c \approx 5.46$, this narrows the range of possible values for $b_G$ to 10 ±1 nm, in good agreement with the estimate given in ref 4. Knowing both $\tau_e/t_c$ and $b_G$ makes it possible to calculate the effect of $SF_6$ on the cation yield. From the photoconductivity studies,[4] it is known that in the presence of $SF_6$ the lifetime of a free electron decreases with $[SF_6]$ as $\tau_e/(1 + \alpha_e[SF_6])$, where the Stern−Volmer constant $\alpha_e \approx 6.7 \times 10^3$ $M^{-1}$. Using this dependence, it is possible to fit the plot of the initial solvent cation yield (Figure 4b) as a function of $[SF_6]$, using a single adjustable parameter: the initial cation yield in neat sc $CO_2$ (see section 2S.2 for more detail). This excellent agreement suggests that our estimate for the electron thermalization distance in radiolysis of sc $CO_2$ is correct.

As discussed in section 3.2, in neat sc $CO_2$, the formation kinetics of the solvent radical cation and the electric field effect on the cation yield are strongly affected by cross recombination of quasifree electrons and the solvent holes. This effect can be simulated, using the lattice Monte Carlo model (section 2S.3) and/or the semianalytical theory (section 2S.2), assuming uniform space distribution of the electron−hole pairs. Though in reality this distribution is not uniform (as these pairs are clustered in radiolytic spurs), *homogeneous* recombination prevails under the conditions of our experiment. The solid lines drawn in Figure 11 are the theoretical predictions for the field effect and the cation formation kinetics obtained using the semianalytical theory of section 2S.2 (the traces obtained by lattice Monte Carlo calculations, section 2S.3, are also shown therein). Note that no model parameters were adjusted in these simulations; the only assumption made (for the comparison with the experimental data) was that the yield of the ionization is 5 electron−hole pairs per 100 eV. Good agreement with experiment further supports our choice for the model parameters.

The estimate of ≈5 (100 eV)$^{-1}$ for the ionization yield can be corroborated by fitting the solvent hole, $\Delta OD_{900}$, and the electric field kinetics, $\chi(t)$, for concentrated $SF_6$ solutions (Figure 21S). Since the geminate recombination and cross recombination of the $F^-$ and $(CO_2)_n^+$ ions occur on the same time scale, lattice Monte Carlo simulations (section 2S.3) were used in these simulations. It turns out that these simulations can pinpoint the ionization yield because the degree by which the cross recombination arrests the development of the field effect strongly

depends on the ion pair concentration and so does the cation yield. Our simulations give an estimate of 5.1 ± 0.1 pairs per 100 eV.

In sum, the model used to simulate time-resolved conductivity in photoionization of sc $CO_2$ solutions can also be used (with slight modifications) to simulate transient absorption kinetics in radiolysis of sc $CO_2$, including the electric field effect on these kinetics. The same set of model parameters for electron and ion dynamics is obtained in both of these experiments.

**4.2. Dissociative Electron Attachment.** In the simulations discussed above, no provision has been made for the occurrence of dissociative electron attachment in the course of ionization. This reaction would lead to rapid formation of the $CO_3^-$ anion. Since this molecular anion has low mobility (as compared to the quasifree electron) a much greater fraction of the geminate $\{CO_3^-\ (CO_2)_n^+\}$ pairs can survive at the end of the radiolytic pulse as compared to the $\{(CO_2)_n^-\ (CO_2)_n^+\}$ pairs. Thus, even if the fraction of the former pairs is small, the increase in the end-of-pulse concentration of the solvent hole could be large. To give an example, our simulations indicate that if 12% of the ionization events resulted in the formation of $CO_3^-$ anions in place of $e_{qf}^-$ the concentration of the solvent hole would increase by 40% (section 2S.3 and Figure 22S). Note that the estimate for the ionization yield in the $SF_6$ solution (section 4.1) is that for the *total* yield, as there should be no difference between the charge separation dynamics for the $\{CO_3^-\ (CO_2)_n^+\}$ and $\{F^-\ (CO_2)_n^+\}$ pairs. Is there any evidence, direct or indirect, that the $CO_3^-$ anions are present in the reaction mixture?

No spectroscopic evidence for the presence of the carbonate radical anion in the reaction mixture was found. This statement, however, is conditional on the assumption that the VIS spectrum of $CO_3^-$ in sc $CO_2$ and the corresponding extinction coefficients are similar to those for aqueous $CO_3^-$ [26] (and $CO_3^-$ centers in carbonate minerals),[27] where this species has been studied previously. As shown in Part 2 of this study,[10] the $X\ ^2B_1 \rightarrow A\ ^2A_1$ band of the $CO_3^-$ anion in the visible is due to trigonal distortion of this $C_{2v}$ symmetric anion; the closer the unique O−C−O angle is to 120°, the weaker the absorption is. In sc $CO_2$, this trigonal distortion is much weaker than in water,[28] where $CO_3^-$ is hydrogen-bonded to the solvent, and $CO_3^-$ in sc $CO_2$ is likely to be a poor light absorber.[10] Gas-phase experiments agree with this theoretical result: the photodestruction cross sections for the $CO_3^-\cdot H_2O$ anion are several times larger than the cross sections for the $CO_3^-\cdot CO_2$ anion.[29] Because $CO_3^-$ is a poor light absorber in sc $CO_2$ and the dissociative electron attachment is a minor channel (as suggested by the simulations in section 2S.3), this species can easily escape detection by transient absorption spectroscopy: The weak absorption of $CO_3^-$ is swamped by much stronger signals from the solvent radical cation, solvent radical anion, and the neutral product. Given that $CO_3^-$ is formed both in the electron bombardment of $(CO_2)_2$ clusters[11] and in $\gamma$-radiolysis of solid $CO_2$,[13] it is likely that this species is also formed in sc $CO_2$, albeit at low yield. There are several reasons to believe that this yield is indeed low other than the fact that the absorbance of $CO_3^-$ was missed in our experiments:

If both $CO_3^-$ and $(CO_2)_n^-$ anions were present in the reaction mixture, there would be no parity between the yields of the solvent radical anion and the solvent radical cation. Figure 7 shows a comparison between the electron photodetachment and absorption spectra of the solvent radical anion. The extinction coefficients $\epsilon^-_\lambda$ for the solvent radical anion were determined using the coefficient $\epsilon^+_\lambda$ obtained in section 3.1, assuming that there is a parity between the ion yields. The cross sections for the electron photodetachment[4] are given as $\epsilon^-_\lambda\ \phi_{pd}$, where $\phi_{pd}$ is the quantum yield of photodetachment. An examination of Figure 7 suggests that $\phi_{pd} \sim 1$ where the comparison is possible. Because the quantum yield of the electron photodetachment cannot exceed unity, there cannot be large deviations from parity provided that our estimates for $\epsilon^+_\lambda$ are correct.

Let us suppose that $\epsilon^+_\lambda$ is underestimated, so that $\phi_{pd} < 1$ ($\epsilon^+_\lambda$ cannot be overestimated as that would require $\phi_{pd} > 1$). In such a case, the parity argument does not apply and some $CO_3^-$ anions could be present in the reaction mixture. Note that the error in $\epsilon^+_\lambda$ cannot be large because kinetic analyses in section 3.1 give a value that is just 20% greater than the estimate obtained in the scavenging experiment. In these kinetic analyses, the quantity determined is the ratio $k_2/\epsilon^+_\lambda$ of the rate constant $k_2$ of ion recombination and the extinction coefficient $\epsilon^+_\lambda$. To obtain $\epsilon^+_\lambda$, the Debye constant was used as an estimate of $k_2$. Because $k_2$ cannot exceed this Debye constant, the error in $\epsilon^+_\lambda$ cannot be greater than 20%. However, this 20% error is unlikely as there would be a conflict with the dosimetry measurement: If slowly recombining geminate $\{CO_3^-\ (CO_2)_n^+\}$ pairs were formed during the ionization, this would increase the apparent prompt yield of the solvent cations because more pairs can be observed on the nanosecond time scale. As explained in sections 3.3 and 1S.2, the yield of the cation absorbance at $\lambda = 900$ nm is 10-to-20% higher than the theoretical estimate after the latter is corrected for the nonuniformity of dose deposition in the sample. If $\epsilon^+_\lambda$ were 20% higher, this discrepancy would disappear, and there would be no room for the increased cation yield that needs be observed when a large fraction of $CO_3^-$ anions is present in the solution.

If our estimate for $\epsilon^+_\lambda$ is correct, this means that the increased yield of the 900 nm absorbance is due to the increased yield of the solvent radical cation (as compared to the theoretical yield obtained in the model without the $CO_3^-$ anions). Monte Carlo calculations indicate that 20% higher end-of-the-pulse cation yield would require 5% of the ionization events to proceed via the formation of $CO_3^-$. Because the field effect in the $\{CO_3^-\ (CO_2)_n^+\}$ pairs is slow to develop, higher fraction of the $CO_3^-$ anion means lower prompt electric field effect. A comparison between the theoretical and experimental values for this field effect brackets the initial fraction of the $CO_3^-$ anions to less than 3%.

In conclusion, though our measurements may be subject to errors, these errors seem to be too small to accommodate large prompt yield of the carbonate radical anion. The highest estimate that can be placed for the prompt yield of this anion is around 10% (relative to the yield of the solvent radical cation) which implies that no more than 2−3% of the ionization events involve dissociative electron attachment.

**4.3. Light-Absorbing Product.** In this section, we make an educated guess as to the possible nature of the neutral product responsible for the long-lived absorption centered at 550 nm. As we do not have evidence that this product is impurity related, we will assume it is not. The following properties were established for this product: The product is extremely stable. It is formed rapidly (in 300 ns) but not promptly. The product is not processed through the electron−hole pair, as there is no prompt electric field effect on its yield. Addition of $H_2$, $N_2O$, $O_2$, and CO (<1 M) does not change the formation kinetics. The product slowly reacts with reducing species ($H_2$ and CO), but it does not react with oxidizing species ($O_2$ and $N_2O$). The latter suggests that the product is in a high oxidation state.

The extremely long lifetime (>300 ms) of the neutral product excludes excited molecular states. Only radicals and ground state

molecules are suitable. The fact that in the high-dose regime the decay kinetics of the product become considerably shorter (section 3.4) suggests that it is a radical that decays by bimolecular recombination. Our search of the literature (e.g., ref 30) suggests that very few neutral, stable $C_xO_y$ species absorbing light in the visible are known. Among the few that we found are "red graphite" (carbon suboxide polymer, $(C_3O_2)_n$),[30,31] singlet carbon trioxide ($CO_3$),[32−39] and ozone ($O_3$).[1,40] Most of the other chromophores (for instance, $C_2O(^3\Sigma)$)[41] can be eliminated on the basis of their short lifetimes and/or low oxidative states. The UV−vis spectrum of "red graphite"[31] has striking resemblance to that of the product. However, it is unclear how such a polymer could be formed on a submicrosecond time scale. The known chemical pathways to this product are thermally induced polymerization of $C_3O_2$[30,31] and prolonged $\gamma$-radiolysis of CO.[42]

*Ozone.* Ozone has the merit of being actually observed in radiolysis of sc $CO_2$.[1,43] It is also generated in 248 nm laser photolysis of $O_2$ in this liquid.[44] Both in radiolysis and photolysis, ozone is formed in the reaction of $O(^3P)$ atoms with $O_2$.[1,12,43,44] Ground-state oxygen atoms do not absorb light in the visible and are stable for tens of microseconds.[1]

There are several reasons to exclude the ozone: $O_3$ does not react with $H_2$ and CO.[45] The visible (Chappius) band of $O_3$ does not match the 550 nm band of the product.[40] The extinction coefficient in the Chappius band is extremely low: in the gas phase, the absorption cross section at the center of this band is just $7 \times 10^{-21}$ cm$^2$.[40a] Though this cross section increases 2−6 times in the condensed media,[40b] one would need the $G$ values in excess of 100 ozone molecules per 100 eV to obtain the observed $G\epsilon^{p}_{550}$ of $\sim$145 M$^{-1}$ cm$^{-1}$ (100 eV)$^{-1}$. A chain reaction could provide large radiolytic yields. However, such a reaction would take a long time, whereas the formation of the product is over in 300 ns. UV absorbance measurements of Dimitrijevic et al.[1] do not support the high yield of $O_3$ in radiolysis of sc $CO_2$ (from Figure 1 in ref 1, we estimate that the $G$ value for ozone is $\approx$0.1 molecule per 100 eV).

*$CO_3$ ($X\ ^1A_1$)* . Carbon trioxide is formed in the reaction of the singlet $O(^1D)$ atom with $CO_2$.[32−37,45] The radical is $C_{2v}$ symmetric, with a three-membered OCO ring and an exocyclic carbonyl group.[34,37,38,39] It is stable both in the gas phase[46] and in low-temperature matrixes.[32−36] $CO_3$ is known to occur in the UV photolysis of $O_3$ in solid,[34,35,36] liquid,[33] and supercritical $CO_2$.[44] In these media, it decays by bimolecular recombination with the formation of $CO_2$ and $O_2$. $CO_3$ does not react with $O_2$ and $O_3$;[32,33] it has been predicted to react with CO (refs 37 and 38 and references therein).

Ab initio calculations[38] suggest that the $X\ ^1A_1$ state absorbs in the visible (2.47 eV) via a transition to the first excited ($A\ ^1B_1$) state; the oscillator strength of 0.03 was obtained for this symmetry-allowed transition. Jones and Taube[32] obtained the VIS spectrum of $CO_3$ by photolysis of $O_3$ in solid $CO_2$ (60−80 K). Their spectrum is similar to the spectrum of the neutral product observed in radiolysed sc $CO_2$ save for a red shift in the latter. A molar extinction coefficient of $\sim$11 M$^{-1}$ cm$^{-1}$ and the oscillator strength of $3 \times 10^{-4}$ were obtained by these authors.[32] In light of the ab initio calculations,[38] their estimate appears to be excessively low, and the VIS spectrum reported by Jones and Taube[32] is in doubt. For $\epsilon^{p}_{550} \sim 10$ M$^{-1}$ cm$^{-1}$, the $G$ value for the product would be $\sim$13.5 radicals per 100 eV which is still too high. However, it seems likely that the actual extinction coefficient for $CO_3$ is at least 10−100 times higher. Admittedly an exotic species, $CO_3$ appears to be the most likely candidate for the light-absorbing product observed in our study. Chemical behavior and light-absorbing properties of $CO_3$ are consistent with this association.

*Formation of $CO_3$.* A possible mechanism for the formation of $CO_3$ in radiolysis of sc $CO_2$ would be the dissociation of $CO_2$* molecules[47] generated either by the direct excitation of the solvent or by charge recombination. The lowest-energy dissociation channels of $CO_2$* are $CO(X\ ^1\Sigma) + O(^1D)$, $CO(X\ ^1\Sigma) + O(^1S)$, and $CO(A^2\Pi) + O(^3P)$ at 7.4, 9.6, and 11.5 eV, respectively.[47a] The $CO(X\ ^1\Sigma) + O(^3P)$ channel (at 5.45 eV) is spin-forbidden.[47a,c] Still, such a dissociation can occur for $CO_2$* molecules generated by the recombination of triplet-correlated electron−hole pairs. In the gas phase, the $O(^1D)$ atoms decay mainly by conversion to ground-state $O(^3P)$ atoms in two-body collisions with $CO_2$ molecules ($2 \times 10^{-10}$ cm$^3$ molecules$^{-1}$ s$^{-1}$).[37,47b] Alternatively, the $O(^1D)$ atom complexes with a $CO_2$ molecule to produce $CO_3(^1A_1)$ in a three body reaction.[46] At 1 bar of He, the complexation is $10^3$ slower than the deactivation.[46] In solid and liquid $CO_2$, the complexation appears to be more efficient.[32,33]

Given that the solvent hole in sc $CO_2$ is a $(CO_2)_2^+$ dimer (with binding energy of 0.6 eV)[48] solvated by the supercritical fluid (which adds −1 eV of the polarization energy), only $CO(X\ ^1\Sigma) + O(^1D,^1S)$ dissociation is possible for $CO_2$* formed by charge recombination. Because $\sim$95% of the electron−hole pairs recombine in less than 50 ps,[4] most recombination events yield singlet $CO_2$* molecules whose dissociation yields *singlet* oxygen atoms. Simpleminded extrapolation of the gas-phase data (at 1 bar) to supercritical fluid (200 bar) suggests that 10−20% of the $O(^1D)$ atoms can yield $CO_3$ instead of converting to $O(^3P)$. Thus, *prompt* formation of $CO_3$ in radiolysis of neat sc $CO_2$ is possible. There could also be delayed formation of this species because of generation of the excited $CO_2$* molecules in recombination of the solvent radical anion and the solvent radical cation in the bulk.

Though plausible, this mechanism is inconsistent with our results: First, the product is formed in a delayed fashion only; there is no prompt formation. Second, when $(CO_2)_n^+$ and $e_{qf}^-$ are scavenged, the formation kinetics of the product do not change. Third, if $CO_3$ were formed in the recombination of the electron−hole pairs, there would be a negative electric field effect on its yield.

We suggest that $CO_3$ is formed by neutralization of $CO_3^-$. In this scenario, the dissociation of $CO_2$* produces relaxed $O(^3P)$ atoms only, and the $CO_3$ radicals are formed via the recombination of cations ($X^+$) with the $CO_3^-$. Because the electric field effect in the $\{CO_3^-\ X^+\}$ pairs takes long time to develop (hundreds of nanoseconds), the field effect on the product yield can be small. $CO_3^-$ does not react with $H_2$, CO, and $N_2O$, and the $O^-$ anion transfer to $O_2$ is very slow ($4 \times 10^6$ M$^{-1}$ s$^{-1}$ in the gas phase).[49] Note that the formation kinetics of $CO_3$ mirror the decay kinetics of $CO_3^-$ which explains the time scale for the delayed generation of the product. As discussed in section 4.2, our results do not exclude that the $CO_3^-$ anion is formed in radiolysis of sc $CO_2$, provided that its initial yield is less than 0.15 per 100 eV. Because all $CO_3^-$ anions will eventually recombine, the yield of $CO_3$ equals this initial yield (this is another reason, why no electric field is observed). Thus, if $CO_3$ has an extinction coefficient of $\sim 10^3$ M$^{-1}$ cm$^{-1}$, there would be sufficient concentration of $CO_3$ to account for the observed product absorbance.

## 5. Conclusion

Using pulse radiolysis−transient absorption spectroscopy, the mechanism for radiolysis of dense, liquidlike supercritical $CO_2$

has been studied ($T = 41$ °C, $\rho/\rho_c = 1.79$). Time-resolved absorption spectra obtained in the 350−1500 nm region are decomposed into the contributions from several species, on the basis of their kinetic behavior, response to the electric field, and reactions with added solutes. Three species have been shown to contribute to the absorption spectra obtained in neat sc $CO_2$: the solvent radical cation, the solvent radical anion, and a long-lived neutral product that we postulate is $CO_3(^1A_1)$. A broad, bell-shaped spectrum of the solvent radical cation centered at 750 nm with an onset at 1.5 $\mu$m and an oscillator strength of 0.153 was isolated. In Part 2 of this series,[10] this spectrum is shown to be due to a charge resonance band[50] of the $(CO_2)_2^+$ core of the solvent hole. A very similar spectrum was obtained for an isoelectronic species,[51] $(N_2O)_2^+$, in sc $CO_2$ (section 3S). The UV−vis absorption spectrum of the solvent radical cation is from a bound-to-continuum electron transition. A comparison between the absorption and electron photodetachment spectra[4] for this anion indicates that the quantum yield of the photodetachment is close to unity.

The following mechanism for electron radiolysis of sc $CO_2$ is suggested: The interaction of the electrons with the solvent causes its ionization with the total yield of $5.1 \pm 0.1$ pairs per 100 eV. Most of these pairs are comprised of the solvent hole and thermalized quasifree electron; the yield of dissociative electron attachment (with the formation of $CO_3^-$ in place of the quasifree electron) is less than 2−3% of the total ion yield. The quasifree electrons are trapped by the solvent in less than 200 ps to yield a solvent radical anion. Because of high electron mobility, most of this trapping occurs after the charges escape each other's Coulomb field. By addition of $SF_6$, it is possible to dramatically shorten the lifetime of the quasifree electron and increase severalfold the yield of the solvent radical cations. For an isolated electron−hole pair, the ratio $\tau_e/t_c$ of the "trapping" time and the Onsager time of the electron−hole pair is $\approx$5.5.[4] Consequently, the electric field effect in such pairs does not develop fully, reaching 40−50% of the maximum theoretical value. Under the conditions of our experiment, there is considerable cross recombination of the quasifree electrons with nongeminate solvent holes that are gradually accumulated in the reaction mixture within the duration of the radiolytic pulse. This cross recombination further shortens the electron lifetime and reduces the electric field effect on the solvent cation yield. We have resolved this process in time and suggested theoretical models to account for the dynamics observed.

The decay kinetics of the solvent radical ions observed on the submicrosecond scale are dominated by two reactions: (i) homogeneous recombination in the bulk and (ii) conversion of the solvent hole to a solute cation, in a scavenging reaction with impurity (most likely, water)[52] and radiolytic products (CO and $O_2$). On the same time scale, the light-absorbing $CO_3$ radical is formed by neutralization of the $CO_3^-$ anion. Because of low yield and poor light absorbance, these $CO_3^-$ anions evade direct detection by transient absorption spectroscopy.

We believe that $CO_3(^1A_1)$ is the most likely candidate for the long-lived light-absorbing product generated in radiolysis of sc $CO_2$. No other intrinsic species has the required combination of chemical and absorption properties. This product exhibits a half-life time of 330 ms, an absorption band centered at 550 nm, and a radiolytic yield $G\epsilon^p{}_{550} \sim 150\ M^{-1}\ cm^{-1}\ (100\ eV)^{-1}$. The proposed mechanism for delayed generation of this product is conditional on several assumptions none of which we can prove: (i) that $CO_3$ has extinction coefficient $\geq 10^3\ M^{-1}\ cm^{-1}$ and a VIS band centered around 550 nm (as suggested by ab initio calculations),[38] (ii) that a low concentration of $CO_3^-$ anions is present in the reaction mixture shortly after the ionization (as suggested by the dose dependencies obtained in section 3.3), (iii) that charge neutralization of $CO_3^-$ yields $CO_3$ radicals, and (iv) that dissociation of $CO_2^*$ molecules formed in the recombination of the electron−hole pairs in sc $CO_2$ yields mainly $O(^3P)$ atoms (as suggested in refs 1 and 2). Disproving any one of these assumption would falsify the suggested mechanism. Although our association of the light-absorbing neutral product with $CO_3$ is tentative, it can be a starting point for further studies. In particular, the IR bands of $CO_3$ in solid matrixes are known,[34,35,36] so that this product could be identified by resonance Raman spectroscopy.

The effect of several scavengers, such as $SF_6$, $H_2$, $O_2$, CO, and $N_2O$ has been studied (section 3S). Radiolysis of their solutions yields many exotic ions that have previously been observed only in the gas phase and in cryogenic matrices. It appears that most di- and triatomic molecules that can donate an electron to the solvent hole form radical cations that rapidly polymerize. The resulting multimer cations exhibit charge resonance bands[50] and can be observed by transient absorption spectroscopy. This finding illustrates the extreme proficiency of sc $CO_2$ to facilitate cationic polymerization.

**Acknowledgment.** We thank Drs. D. M. Bartels, N. M. Dimitrijevic, and A. D. Trifunac for many stimulating discussions and Dr. S. D. Chemerisov for the operation of the linac. This work was performed under the auspices of the Office of Basic Energy Sciences, Division of Chemical Science, US-DOE under Contract No. W-31-109-ENG-38.

**Supporting Information Available:** (1.) Experimental setup and procedures; (2.) Appendix: Electric field effect on the solvent cation yield; (3.) Scavenging experiments with $O_2$, $N_2O$, and CO; (4.) Additional references; (5.) Captions to Figures 1S to 43S; (6.) Figures 1S−43S. This material is available free of charge via the Internet at http://pubs.acs.org.

## References and Notes

(1) Dimitrijevic, N. M.; Bartels, D. M.; Jonah, C. D.; Takahashi, K. *Chem. Phys. Lett.* **1999**, *309*, 61.

(2) Dimitrijevic, N. M.; Takahashi, K.; Bartels, D. M.; Jonah, C. D.; Trifunac, A. D. *J. Phys. Chem. A* **2000**, *104*, 568.

(3) Takahashi, K.; Sawamura, S.; Dimitrijevic, N. M.; Bartels, D. M.; Jonah, C. D. *J. Phys. Chem. A* **2002**, *106*, 108.

(4) Shkrob, I. A.; Sauer, M. C., Jr. *J. Phys. Chem. B* **2001**, *105*, 4520.

(5) Itoh, K.; Holroyd, R. A.; Nishikawa, M. *J. Phys. Chem. A* **2001**, *105*, 703.

(6) Bowen, K. H.; Eaton, J. G. In *The Structure of Small Molecules and Ions*; Naamna, R., Vagar, Z., Eds.; Plenum: New York, 1987; p 147. DeLuca, M. J.; Niu, B.; Johnson, M. *J. Chem. Phys.* **1988**, *88*, 5857. Tsukuda, T.; Johnson, M.; Nagata, T. *Chem. Phys. Lett.* **1997**, *268*, 429.

(7) Holroyd, R. A.; Gangwer, T. E.; Allen, A. O. *Chem. Phys. Lett.* **1975**, *31*, 520. Lukin, L. V.; Yakovlev, B. S. *High Energy Chem.* **1978**, *11*, 440.

(8) Saeki, M.; Tsukuda, T.; Iwata, S.; Nagata, T. *J. Chem. Phys.* **1999**, *111*, 6333.

(9) Zhou, M.; Andrews, L. *J. Chem. Phys.* **1999**, *110*, 6820. Zhou, M.; Andrews, L. *J. Chem. Phys.* **1999**, *110*, 2414. Thompson, W. E.; Jacox, M. E. *J. Chem. Phys.* **1999**, *111*, 4487; *J. Chem. Phys.* **1989**, *91*, 1410.

(10) Shkrob, I. A. *J. Phys. Chem. A* **2002**, *106*, 11871.

(11) Klots, C. E.; Compton, R. N. *J. Chem. Phys.* **1978**, *69*, 1636.

(12) (a) Kummler, R.; Leffert, C.; Im, K.; Piccirelli, R.; Kevan, L.; Willis, C. *J. Phys. Chem.* **1977**, *81*, 2451. (b) Yoshimura, M.; Chosa, M.; Soma, Y.; Nishikawa, M. *J. Chem. Phys.* **1972**, *57*, 1626. (c) Harteck, P.; Dondes, S. *J. Chem. Phys.* **1957**, *26*, 1727; *J. Chem. Phys.* **1955**, *23*, 9029. (d) Karasawa, H.; Yugeta, R.; Yamaguchi, A.; Sato, S. *Bull. Chem. Soc. Jpn.* **1981**, *54*, 362.

(13) Hirai, M.; Ikeya, M.; Tsukamoto, Y.; Yamanaka, C. *Jpn. J. Appl. Phys.* **1994**, 55, L1453. Tsukamoto, Y.; Ikeya, M.; Yamanka, C. *Appl. Radiat. Isot.* **1993**, *44*, 221; **2000**, *52*, 1259. Wu, G. *Appl. Radiat. Isot.* **2001**, *55*, 895; Norizawa, K.; Kanosue, K.; Ikeya, M. *Appl. Radiat. Isot.* **2001**, *55*, 896.

(14) Cooper, H. W.; Goldfrank, J. C. *Hydrocarbon Process. Petrol. Refiner* **1967**, *46*, 141. Moriyoshi, T.; Kita, T.; Uosaki, Y. *Ber. Bunsen-Ges. Phys. Chem.* **1993**, *97*, 589.

(15) Schuler, R. H.; Patterson, L. K.; Janata, E. *J. Phys. Chem.* **1980**, *84*, 2089. Buxton, G. V.; Stuart, C. R. *J. Chem. Soc., Faraday Trans.* **1995**, *91*, 279.

(16) In this optical time-of-flight experiment, the loss of the ions because of their discharge at the electrodes is observed. Under our experimental conditions, the drift of the ions is stalled by the space charge in the sample (see ref 21). Assuming that the ions do not recombine, we found, by numerical simulations, that for an initial ion concentration of 1 $\mu$M and a field of 25 kV/cm ca. 20% of the ions will be neutralized at the electrodes at $t = 5$ ms (for typical ion mobilities of $\mu_+ = 2 \times 10^{-3}$ cm$^2$/Vs and $\mu_- = 4 \times 10^{-3}$ cm$^2$/Vs, ref 4). For an initial concentration of 100 nM, the same fraction of ions will be neutralized at 2 ms; the lower the concentration, the faster the ion decay. Because we have not observed any field-induced loss of the 550 nm absorbance on the 1−100 ms time scale, the conclusion is that the product is not an (unusually stable) ion.

(17) For example, see: Shkrob, I. A.; Sauer, M. C., Jr.; Trifunac, A. D. *J. Phys. Chem.* **1996**, *100*, 5993; *J. Phys. Chem.* **1996**, *100*, 7237; *J. Phys. Chem.* **1996**, *100*, 6876.

(18) Mehnert, R.; Brede, O.; Naumann, W. *Ber. Bunsen-Ges. Phys. Chem.* **1984**, *88*, 71.

(19) We used several other common electron scavengers, such as $O_2$, $CH_2Cl_2$, and $CCl_4$, without success: $CO_4^-$ efficiently reduces aromatic solutes, whereas the addition of halocarbons yields strong absorbance bands from their radical cations.

(20) Warman, J. M.; Asmus, K. D.; Schuler, R. H. *J. Phys. Chem.* **1969**, *73*, 931.

(21) Hummel, A.; Schmidt, W. F. *Radiat. Res. Rev.* **1974**, *5*, 199.

(22) Hong, K. M.; Noolandi, J. *J. Chem. Phys.* **1978**, *69*, 5026. Onsager, L. *Phys. Rev.* **1938**, *54*, 554.

(23) Mozumder, A. *J. Chem. Phys.* **1974**, *61*, 780; *J. Chem. Phys.* **1968**, *48*, 1659.

(24) For example, see: Bullot, J.; Cordier, P.; Gauthier, M. *J. Phys. Chem.* **1980**, *84*, 1253.

(25) Because of a calculation error, the product $G\epsilon_{750}$ given in refs 1 and 2 is two times greater than the correct value.

(26) Weeks, J. L.; Rabani, J. *J. Phys. Chem.* **1966**, *70*, 2100. Behar, D.; Czapski, G.; Duchovny, I. *J. Phys. Chem.* **1970**, *74*, 2206

(27) Chantry, G. W.; Horsfield, A.; Morton, J. R.; Whiffen, D. H. *Mol. Phys.* **1962**, *5*, 589. Serway, S. R. A.; Marshall, S. A. *J. Chem. Phys.* **1967**, *46*, 1949.

(28) Hiraoka, K.; Yamabe, S. *J. Chem. Phys.* **1992**, *97*, 643.

(29) Snodgrass, J. T.; Kim, H.-S.; Bowers, M. T. *J. Chem. Phys.* **1988**, *88*, 3072. Roehl, C.; Snodgrass, J. T.; Deakyne, C. A.; Bowers, M. T. *J. Chem. Phys.* **1991**, *94*, 6546. Smith, G. P.; Lee, L. C.; Moseley, J. T. *J. Chem. Phys.* **1979**, *71*, 4034.

(30) Gmelin, L.; et al. *Gmelins Handbuch Der Anorganishen Chemie*; Verlag Chemie: Leipzig-Berlin, 1970; v. 14.C.1, pp 70−97.

(31) Smith, R. N.; Young, D. A.; Smith, E. N.; Carter, C. C. *Inorg. Chem.* **1963**, *2*, 829.

(32) Jones, P. R.; Taube, H. *J. Phys. Chem.* **1971**, *75*, 2991.

(33) DeMore, W. B.; Jacobsen, C. W. *J. Phys. Chem.* **1969**, *73*, 2935.

(34) Jacox, M. E.; Milligan, D. E. *J. Chem. Phys.* **1971**, *54*, 919.

(35) Moll, N. G.; Clutter, D. R.; Thompson, W. E. *J. Chem. Phys.* **1966**, *45*, 4469.

(36) Weissberger, E.; Breckenridge, W. H.; Taube, H. *J. Chem. Phys.* **1967**, *47*, 1764.

(37) Froese, R. D. J.; Goddard, J. D. *J. Phys. Chem.* **1993**, *97*, 7484.

(38) Castro, M. A.; Canuto, S.; Simas, A. M. *Chem. Phys. Lett.* **1991**, *177*, 98. Canuto, S.; Diercksen, G. H. F. *Chem. Phys.* **1988**, *120*, 375.

(39) LaBonville, P.; Kugel, R.; Ferraro, J. R. *J. Chem. Phys.* **1977**, *67*, 1477.

(40) (a) Griggs, M. *J. Chem. Phys.* **1968**, *49*, 857. (b) Vaida, V.; Donaldson, D. J.; Strickler, S. J.; Stephens, S. L.; Birks, J. W. *J. Phys. Chem.* **1989**, *93*, 506.

(41) Willis, C.; Devillers, C. *Chem. Phys. Lett.* **1968**, *2*, 51.

(42) Anderson, A. R.; Best, J. V. F.; Willett, M. J. *Trans. Faraday Soc.* **1966**, *62*, 595.

(43) Willis, C.; Binder, P. E. *Can. J. Chem.* **1970**, *48*, 3463.

(44) Otomo, J.; Oshima, Y.; Takami, A.; Koda, S. *J. Phys. Chem. A* **2000**, *104*, 3332.

(45) Harteck, P.; Dondes, S. *J. Chem. Phys.* **1957**, *26*, 1734.

(46) DeMore, W. B.; Dede, C. *J. Phys. Chem.* **1970**, *74*, 2621. Young, R. A.; Ung, A. Y.-M. *J. Chem. Phys.* **1965**, *44*, 3038.

(47) (a) Welge, K. H.; Gilpin, R. *J. Chem. Phys.* **1971**, *54*, 4224. (b) Slanger, T. G.; Sharpless, R. L.; Black, G. *J. Chem. Phys.* **1977**, *67*, 5317. Gentieu, E. P.; Mentall, J. E. *J. Chem. Phys.* **1973**, *58*, 4803. (c) Shaw, D. A.; Holland, D. M. P.; Hayes, M. A.; MacDonald, M. A.; Hopkirk, A.; McSweeney, S. M. *Chem. Phys.* **1995**, *198*, 381 and references therein.

(48) Illies, A. J.; Jarrold, M. F.; Wagner-Redeker, W.; Bowers, M. T. *J. Phys. Chem.* **1984**, *88*, 5204. Kim, H.-S.; Jarrold, M. F.; Bowers, M. T. *J. Chem. Phys.* **1986**, *84*, 4882. Johnson, M. A.; Alexander, M. L.; Lineberger, W. C. *Chem. Phys. Lett.* **1984**, *112*, 285. Illies, A. J.; McKee, M. L.; Schlegel, H. B. *J. Phys. Chem.* **1987**, *91*, 3489. Illies, A. J. *J. Phys. Chem.* **1988**, *92*, 2889. Misev, L.; Illies, A. J.; Jarrold, M. F.; Bowers, M. T. *Chem. Phys.* **1985**, *95*, 469.

(49) Dotan, I.; Davidson, J. A.; Streit, G. E.; Albritton, D. L.; Fehsenfeld, F. C. *J. Chem. Phys.* **1977**, *67*, 2874.

(50) Brocklehurst, B. *Nature* **1968**, *219*, 263. Badger, B.; Brocklehurst, B. *Trans. Faraday Soc.* **1969**, *65*, 2582; *Trans. Faraday Soc.* **1970**, *66*, 2939.

(51) McKee, M. L. *Chem. Phys. Lett.* **1990**, *165*, 265.

(52) Actually $(CO_2)_n^-$ can also react with water impurity, forming a weakly bound complex (see Shkrob, I. A.; Sauer, M. C., Jr. *J. Phys. Chem. B* **2001**, *105*, 7027). However, at low concentration of water, the complexation equilibrium is completely shifted towards the $(CO_2)_n^-$ anion, and the reaction has no effect on the transient absorption kinetics.

(53) Lias, S. G.; Bartmess, J. E.; Liedman, J. F.; Holmes, J. L.; Levin, R. D.; Mallard, W. G. *Gas-Phase Ion Neutral Thermochem., J. Phys. Chem. Ref. Data* **1988**, *17*, Supplement No. 1.